UNIVERSITY OF OKLAHOMA

GRADUATE COLLEGE

DESIGN OF A CIRCULARLY POLARIZED RECTIFYING ANTENNA ON A FLEXIBLE SUBSTRATE AT X-BAND

A THESIS

SUBMITTED TO THE GRADUATE FACULTY

in partial fulfillment of the requirements for the

Degree of

MASTER OF SCIENCE

By

CHRISTOPHER WALKER
Norman, Oklahoma
2019

DESIGN OF A CIRCULARLY POLARIZED RECTIFYING ANTENNA ON A FLEXIBLE SUBSTRATE AT X-BAND

A THESIS APPROVED FOR THE
SCHOOL OF ELECTRICAL AND COMPUTER ENGINEERING

BY THE COMMITTEE CONSISTING OF

Dr. Jay McDaniel, Chair

Dr. Hjalti Sigmarsson

Dr. Jessica Ruyle

This work is dedicated to my mother and father

Acknowledgments

This work would not have been possible without the contribution of Dr. McDaniel, Dr. Sigmarsson and Dr. Ruyle. I would also like to thank all my friends at the Advanced Radar Research Center and the University of Oklahoma. Boomer Sooner.

Table of Contents

List of Figures

Abstract

This thesis lays out the design procedure for a left-hand circularly polarized, high-efficiency rectifying antenna on a flexible substrate for use at 10 GHz. The rectenna system is designed for space based power applications. The rectenna employs a dual rhombic loop antenna to achieve circular polarization with an axial ratio of less than 2 dB. The design is milled on a 100 micron thick DuPont Pyralux TK substrate with $\epsilon_r = 2.5$. A lowpass filter is integrated into the coplanar stripline transmission line to suppress the re-radiated harmonics generated by the rectifier circuit. An RF-to-DC conversion efficiency of 58% is achieved. To the author's knowledge, this is the first rectenna designed on a flexible substrate at X-Band.

Chapter 1

Introduction

1.1 Overview

It has long been a goal of humanity to harness energy for our own technological benefits helping to render our daily lives more comfortable. As centuries have past, different, more sophisticated fuels have provided a corresponding evolution in available energy levels. In 2018, about 4.17 trillion kWh of electricity was generated at utility scale electricity generation facilities. About 64% of this electricity generation was from unsustainable fossil fuel sources (coal, natural gas, petroleum and other gases) [1]. This energy need is constantly growing, calling for safe, reliable and clean alternative energy sources.

Up until the industrial revolution, all our energy came from renewable resources - biomass, wind, water, etc. The development of the 19th century was primarily based on coal burning to produce heat, steam and drive machinery. While at its beginning, 80% of our energy came from renewables and only 20% came from fossil fuels, these numbers completely reversed with the industrial revolution. At the end of WWI almost 80% of energy came from coal combustion, steadily increasing through the 20th century led by the transportation industry. Modern industrial and material processing has brought about a ne-

cessity for denser forms of energy provided by oil, gas and nuclear energy. Over the course of the 20th century, world population has quadrupled and power consumption has increased sixteen fold. Long term, sustainable power sources must be abundant, affordable and clean. With current technology, only one option fulfills all these requirements - the sun [2].

The sun is the most powerful and safe natural fusion reactor we have at our disposal. However, using direct solar irradiation on earth is subject to weather conditions and the natural day-night cycle. This minimizes its use for power generation depending on the location on earth. In outer space, the sun's energy is not attenuated by the atmosphere and up to 60% more power can be received [3]. We can take advantage of space's permanent insulation, lack of weather effects and constant sunlight to produce abundant power for terrestrial needs. The idea is simple; capture solar energy, convert it to a transportable form, and deliver it to where power is needed. A modern approach is to capture the energy, convert it to microwave frequencies, and "beam" it to its final destination where a rectifying antenna (rectenna) down-converts the microwave signal to DC.

1.2 History of the Rectenna

Around the turn of the 20th century, the first investigations of wirelessly transmitting power around the world began. It was the dream of Nikola Tesla to distribute power wirelessly and in large quantities to the most remote locations around the world. In 1899, he used electrical oscillators at 100 MV and 150 kHz to direct uncollimated radiated electromagnetic energy at a lightbulb less than a meter away [4]. Unfortunately, Tesla would go broke before his dreams could ever be realized. Tesla knew power could be transmitted across large

distances, he was simply limited by the technology of his time.

In the 1950s this dream was revived. Goubau and Schwering, among others, demonstrated that wireless power could be transmitted in the far-field using microwave radiation at efficiencies approaching 100% given a "beam waveguide" consisting of focusing lenses and mirrors [5]. This was a landmark discovery as up until this point, it was believed that wireless power density *always* decayed according to the inverse square law. In 1959, the United States Department of Defense (DoD) sparked even more interest in wireless power transmission by promoting the Raytheon Airborne Microwave Platform (RAMP). The project proposed a helicopter, powered by microwave radiation, to be flown at 50,000 feet and allow for over-the-horizon communication systems (a modern solution was the communication satellite). The program would fall short due to the lack of high power microwave tubes needed on the transmit side of the system, as well as a lack of efficient rectifier diodes [6].

In 1964, the father of modern wireless power transmission, William Brown demonstrated a microwave-powered helicopter [7]. This was the first example of the rectenna, which used an array of dipole antennas to receive a 2.4 GHz continuous wave (CW) beam and rectify the power at 55% efficiency outputting 270 Watts. The rectenna was patented by Brown shortly after the success of his microwave powered helicopter in 1969 [8]. Shortly after Brown's microwave powered helicopter milestone, Peter Glaser submitted his patent for gathering and transforming solar radiation to microwaves and beaming that power to a rectenna array on Earth [9]. Glaser's concept would become known as the Space Solar Power Satellite system (SSPS).

In 1985, the first unmanned, fixed wing aircraft powered by microwave was flown by the Stationary High Altitude Relay Program (SHARP) [10]. SHARP

used an 80 meter diameter array of parabolic reflector antennas to beam 500 kW of power to the aircraft at 5.8 GHz. The attached rectenna was a circular microstrip patch antenna used for dual polarization reception. A small scale version of SHARP was flown over the Canadian country side before the aircraft was attacked by field mice in storage and the program was abandoned by the Communications Research Center of Canada.

One of the more recent and impactful designs in rectenna technology came from James McSpadden during his time at Texas A&M University. In 1998, McSpadden et al. used a dipole antenna and filter circuitry on a thin duroid substrate to achieve an RF-to-DC conversion efficiency of 82% at low input power levels of 50 mW [11]. The design was improved by the derivations of Yoo and Chang who put forth closed-form equations for the basic circuit structure of the rectenna [12] as well as the first use of 3D full-wave electromagnetic modeling software in designing a rectenna. Prior to this point, rectennas had been designed using simple transmission line models.

In 2002, Strassner and Chang designed the first circularly polarized rectenna array which took advantage of a high gain antenna in order to minimize the number of elements needed in the array. Their design used coplanar stripline (CPS) transmission line technology to feed dual rhombic loop antennas. Their research achieved 80% conversion efficiency at low input powers [13]. The design of this thesis is based off of the work by Strassner and Chang.

1.3 Motivation

The motivation for this work is to present a novel rectenna design for use with the SSPS system. When designing a component for space-based systems, cost, size, weight and power (C-SWaP) limitations must be considered. According

to the National Aerospace and Space Administration, every pound of payload costs an extra $10,000 to put into orbit. Some of the heaviest components put into space-based systems are power generators (batteries, solar panels, etc.). The rectenna is a great alternative and can allow for two-way power beaming allowing one platform to generate power for multiple systems, or even for downlinking power from space to earth.

A great way to decrease the size and weight of a rectenna system is to use a thin, flexible substrate. These types of substrates are inherently low weight and provide the ability to conform, bend or roll into any shape. Should the rectenna be used on a satellite platform, the flexible substrate would allow the component to be folded away into a fairing during launch, and then folded out when in orbit. These types of substrates are easy to pattern and durable enough to stand the rigors of rocket launches. The substrate used herein is a Kapton-Teflon composite from DuPont called Pyralux TK (model TK 1210012). This substrate is 100 micron thick with a permittivity of 2.5 at 10 GHz and 12 micron of copper on top and bottom. Pyralux TK is also highlighted as a notable material for this work as it has an incredibly low loss tangent of 0.002. This is especially important in power conversion applications as a low loss tangent allows for high conversion efficiencies when dealing with very low power densities seeing as it minimizes the losses between elements in the rectenna and the diode.

This work will also seek to take advantage of a circularly polarized antenna. Since the system should be implemented in space, the orientation between the transmit and receive platforms will not always be controllable. Circular polarization allows the rectenna to maintain a constant DC output voltage regardless of orientation mismatch. It is also interesting to note that

in traditional linearly polarized RF systems, the ionosphere can cause severe attenuation of electromagnetic signals. This effect can be completely ignored when using a circularly polarized receiving antenna.

Chapter 2

Wireless Power Transmission

2.1 Wireless Power Transmission

Wireless power transmission (WPT) systems consist of transmit and receive components which seek to send energy from one point to another via time-varying electromagnetic fields. This type of technology can help eliminate the need for wires and batteries which can be inconvenient and damaging to the environment, as well as allow for power systems to exist and function in remote and rural areas. WPT is divided into two specific categories: near field and far field. The work herein will focus on far field WPT specifically in the form of the rectifying antenna (rectenna).

WPT systems are comprised of three main sections as seen in Figure 2.1: the transmission block functions to convert electrical energy (direct current (DC) or alternating current (AC)) into RF energy. The energy is transmitted through a transmit antenna (Tx) and radiated as a microwave beam through the second section, known as the "free space channel." The final block, known as the receiving block, captures the radiated energy with a receive antenna (Rx) and passes it through a rectifier circuit to convert the signal from RF to DC power.

Each channel has an associated efficiency (η) which is essentially equal to the channel's transfer function; that is the ratio of output power (P_{out}) over input power (P_{in}).

$$\eta = P_{out}/P_{in} \tag{2.1}$$

Multiplying the efficiencies of each respective channel, the overall efficiency of a DC-to-DC WPT system can be computed as follows:

$$\eta_{total} = \eta_t \cdot \eta_c \cdot \eta_r \tag{2.2}$$

Where η_t represents the electric-to-microwave conversion efficiency (transmitter efficiency), η_c represents the efficiency of the free-space channel (collection efficiency), and η_r represents the microwave-to-electric conversion efficiency (rectenna efficiency or receiver efficiency). Each of these three efficiencies can be further broken down into "subefficiencies" where η_t is the product of the efficiency with which DC or AC power is converted into microwave power by an electronic oscillator (such as a magnetron) and the radiation efficiency of the transmit antenna. The collection efficiency, η_c, is simply broken down into the

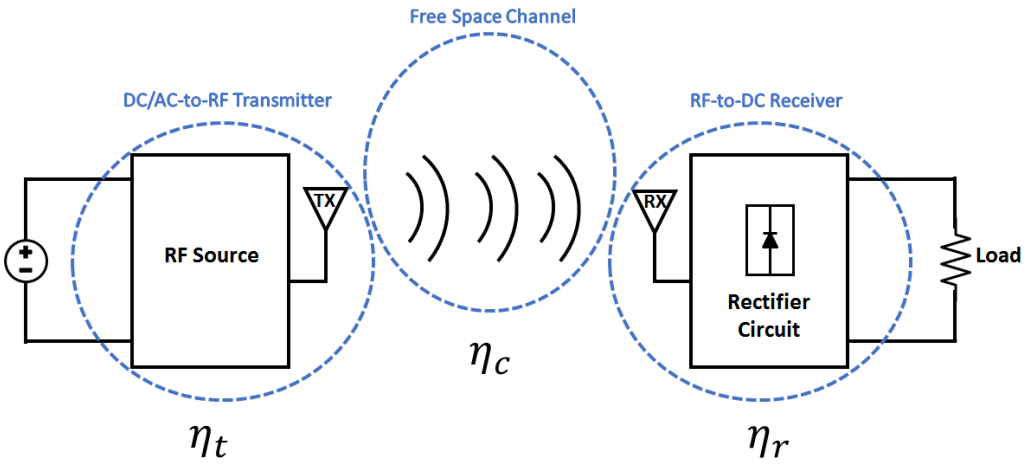

Figure 2.1: WPT Block Diagram

power received over the power transmitted. The rectenna efficiency consists of two parts: 1) the absorption efficiency, or how much of the incident power on the antenna is absorbed into the receiving structure (assuming the antenna is a reciprocal structure this is the same as radiation efficiency); and 2) the conversion efficiency, which is the ratio of rectified DC power on the output of the rectenna to the microwave power into the rectenna. The rectenna structure should consist of uniformly distributed rectifying elements over the receiving structure so that the RF energy captured on an area is immediately converted back into DC power.

In [14], the author lists six advantages resulting from handling the collection and rectification of WPT using a rectenna: 1) the receiving surface has little directivity and need not be precisely pointed at the transmitter; 2) the mechanical tolerances in the construction of the receiving aperture are very relaxed; 3) the problem of matching the illumination pattern established by the incoming radiation to the radiation pattern of a conventional receiving antenna is eliminated; 4) nonuniform intensity and phase illumination of the receiving aperture, which will result from a combination of a very large receiving aperture and nonuniform atmospheric conditions over the cross section of the incoming beam, cause no problems; 5) there is a good match between the amount of microwave power that is received in local regions of the receiving aperture to the power handling capability of solid state microwave rectifiers; and 6) any heat resulting from inefficient rectification in the rectifiers can be easily disposed of in the local region of the receiving aperture.

Chapter 3

Rectenna Theory and the Basics of Rectification

3.1 Introduction to the Rectenna

Just as the name seems to imply, the rectenna is a combination of two different electronic components: the "rectifier" and the "antenna". To convert power from RF to DC, the rectenna should satisfy the following criterion: (1) the effective aperture of the receiver should be relatively large, (2) the rectifying circuit should be capable of handling high power, (3) the antenna pattern should be non-directive, (4) the rectifying circuit should be highly efficient, (5) the rectenna should operate over a substantial frequency range, (6) the element should be light weight, (7) the component should be easy to integrate with mechanical systems, (8) the part should be highly reliable and have a long operating life, (9) it should cause minimal radio frequency (RF) interference [15].

The principle elements that make up the rectenna in this work, which can be seen in Figure 3.1, are the antenna, lowpass filter, rectifier, RF Block/DC pass filter and the resistive load. Each of these elements provide a certain function which ultimately converts the RF power into direct current (DC). The antenna receives radiated power at high frequency and sends the power to the

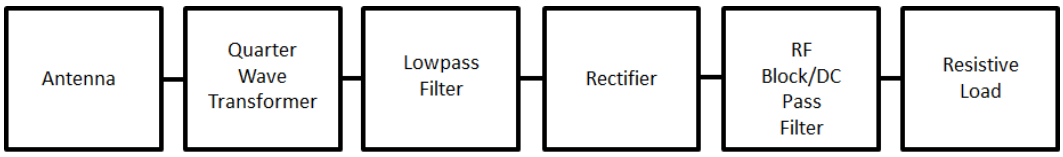

Figure 3.1: Rectenna Block Diagram

lowpass filter. The lowpass filter rejects higher-order harmonics, generated due to the non-linearities of the diode, from being re-radiated into the environment. The quarter-wave transformer exists to transform the impedance of the antenna to the rectifier impedance (note that the lowpass filter is designed to the same impedance as the input side of the diode). The rectifier is the core element of the rectenna and exists to efficiently convert the RF/AC signal to DC power. The RF block/DC pass filter, made up of a large capacitor, has two duties: (1) it ensures that only DC power is transferred to the load resistor by shorting all RF energy back to the rectifier for remixing, (2) the capacitor smooths the DC ripple on the output of the diode.

Before examining each specific piece of the rectenna, it is first important to understand how the half-wave rectifier and the peak half-wave rectifier operate.

3.2 Rectifier Circuits

Figure 3.2(a) shows the circuit schematic for the simple half-wave rectifier. The diode conducts only for the positive half of the input voltage signal that is greater than the diode's DC operating point (V_D); thereby cutting off the negative half of the sinusoid and resulting in a purely positive output signal, as seen in Figure 3.2(a). If the input voltage is of the form $v_s sin(\omega t)$ then the average DC diode current $I_{D_{avg}}$ can be found by integrating the signal over the

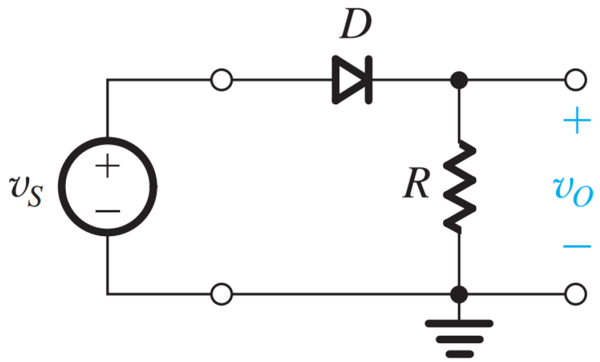

(a) Half-Wave Rectifier Circuit

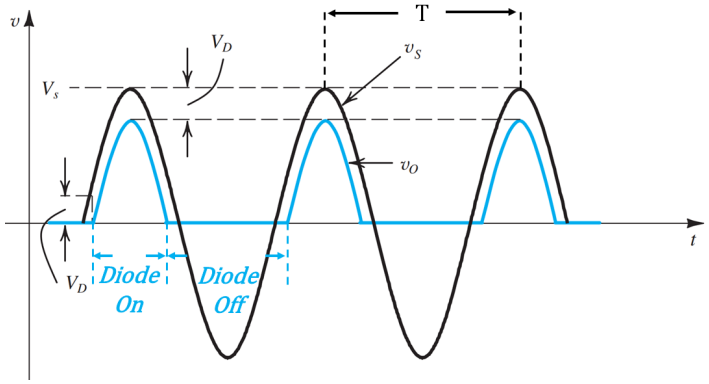

(b) Half-Wave Rectifier Input/Output Waveform

Figure 3.2: The Half-Wave Rectifier [16]

half of the period where the voltage conducts and dividing by the full period:

$$I_{D_{avg}} = \frac{1}{T}\left(\int_0^{T/2} \frac{v_s}{R} sin\ \omega t\ dt\right) \tag{3.1}$$

where T is the period and the frequency $\omega = 2\pi/T$. The solution to (3.1) gives $I_{D_{avg}} = v_s/\pi R$ or $v_{o_{avg}} = v_s/\pi$, which is the average voltage across the load resistor after the diode rectifies the signal. The circuit of Figure 3.2(a) is a nice start, but the variation can be reduced by smoothing the output signal with the use of a filter capacitor as seen in Figure 3.3(a). This circuit is called the peak half-wave rectifier.

The peak half-wave rectifier operates by charging the shunt capacitor when

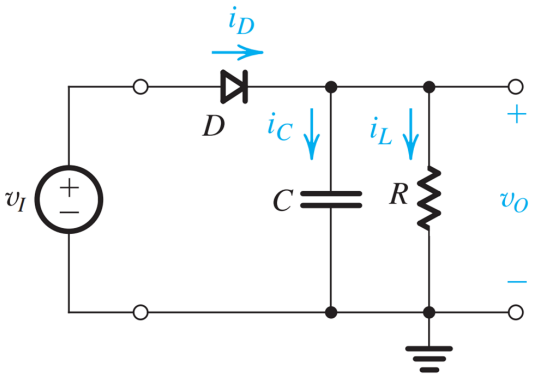

(a) Peak Half-Wave Rectifier Circuit

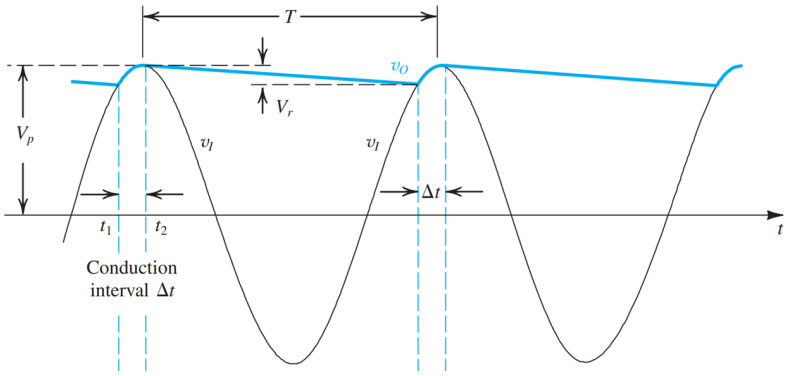

(b) Peak Half-Wave Rectifier Input/Output Waveform

Figure 3.3: The Peak Half-Wave Rectifier [16]

the diode is conducting. When the diode turns off, the capacitor will slowly discharge it's stored energy resulting in a voltage waveform that approaches the peak voltage of the input signal V_p. This can only hold true if the circuit's RC time constant is much greater than the period of the input signal, i.e. $RC >> T$. The input and output voltage waveforms can be seen in Figure 3.3(b). During the time which the diode is off, the capacitor is discharging and the equation that represents a discharging capacitor can be seen in (3.2).

$$V_c(t) = V_p \, e^{\frac{-t}{RC}} \tag{3.2}$$

The capacitor discharges until the diode conducts again, the time for which

can be approximated to be the full period T. Thus, the voltage across the load after the period of discharge can be represented by (3.3).

$$v_{o_{min}} = V_p - V_r \approx V_p \; e^{\frac{-T}{RC}} \tag{3.3}$$

$$V_r \approx V_p \; (1 - e^{\frac{-T}{RC}}) \tag{3.4}$$

This can be simplified by using the Taylor Series Expansion for $e^{\frac{-T}{RC}} = 1 - \frac{T}{RC} - \frac{\frac{T}{RC}}{2!} - ...$ and the fact that $RC >> T$ to get (3.5).

$$V_r \approx V_p \; (1 - (1 - \frac{T}{RC})) \approx V_p \; \frac{T}{RC} \tag{3.5}$$

Equation (3.5) can be expressed in terms of frequency using $T = 1/f$ giving

$$V_r = \frac{V_p}{fRC} \tag{3.6}$$

and thus in order to maintain a small ripple voltage V_r, a capacitance value C that ensures that $RC >> T$ must be chosen.

3.3 Building a Model for Diode Efficiency and Input Impedance

The most important component operating within the rectenna system is the diode. The properties and operations of diodes have been studied at great length. In [12], the authors put forward the derivation of a closed-form equation for the conversion efficiency of a schottky diode at high frequency used for a rectenna. The derivation stands on the following assumptions: the applied RF voltage across the diode consists of only the DC term and the fundamental

frequency component; the current due to the junction capacitance is negligible when the diode is forward biased; the junction resistance is infinite when the diode is off; the forward voltage drop across the intrinsic diode junction is constant during the forward-bias period; the phase delay between the input RF voltage wave and the diode junction voltage wave is zero; and temperature effects are negligible [17]. Figure 3.4 shows an incident RF waveform (V_I) and the corresponding junction voltage waveform (V_j) operating upon the circuit model in Figure 3.5. Since the fundamental frequency component of the voltage wave is not corrupted by higher order harmonic components, the rectenna conversion efficiency strongly depends on the characteristics of the diode.

The voltage waveform is expressed as

$$V_I = -V_D + V_P \; cos(\omega t) \tag{3.7}$$

where V_D represents the self-bias DC output voltage across the resistive load R_L, and V_P represents the peak voltage amplitude of the incident RF power. The diode junction voltage is represented by V_j and can be expressed by (3.8)

$$V_j = \begin{cases} -V_{j0} + V_{j1} cos(\omega t - \phi) & V_j < V_{bi} \text{ diode is off} \\ V_{bi} & V_j \geq V_{bi} \text{ diode is on} \end{cases} \tag{3.8}$$

where V_{j0} represents the diode's junction voltage at DC, and V_{j1} represents the diode's junction voltage at the fundamental frequency. V_{bi} represents the diode's bias voltage, or built-in forward turn-on voltage. θ_{on} represents the forward bias turn-on angle. The diode is considered to be forward-conducting when the junction voltage V_j is greater than the bias voltage. Note the diode's junction waveform slightly lags the incident power by the phase difference ϕ.

Figure 3.5 portrays an equivalent circuit model of the half-wave rectifier. The model consists of a diode series resistance R_S, a nonlinear junction resistance R_j, a non-linear junction capacitance C_j, and a load resistor R_L. When the diode conducts, R_j is assumed to be zero, when the diode is non-conducting we consider R_j to be infinite. Using basic circuit analysis, it can be shown that

$$V_D + I_D R_S + V_{j,dc} = 0. \tag{3.9}$$

Setting $I_D = \frac{V_D}{R_L}$, the DC output voltage across the load is given by

$$V_D = -V_{j,dc} \frac{R_L}{R_S + R_L}. \tag{3.10}$$

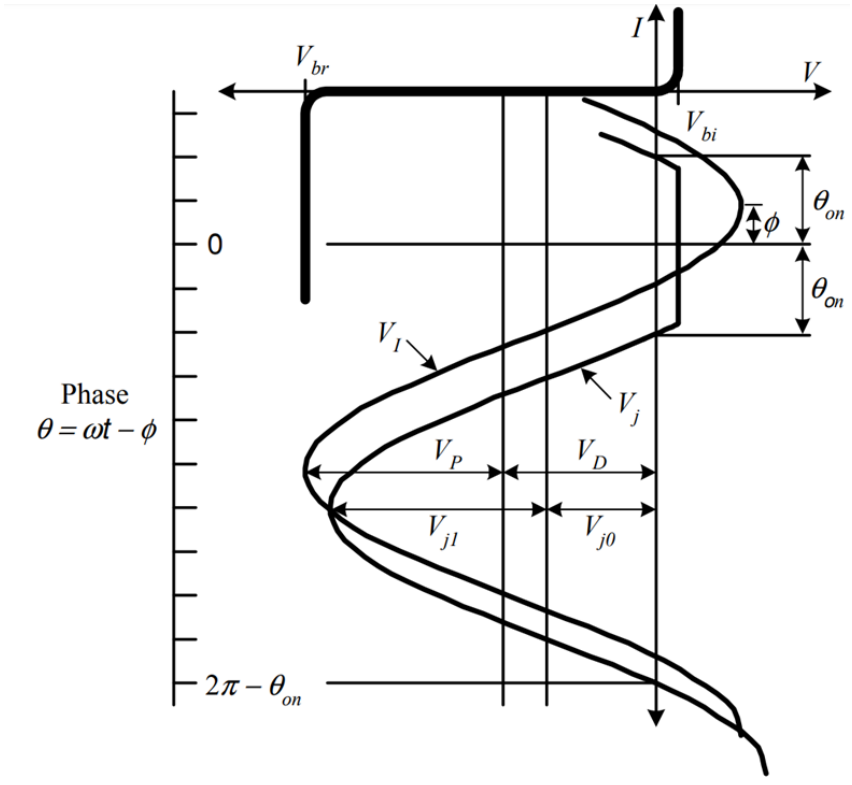

Figure 3.4: Diode I-V characteristic curves with the incident RF voltage waveform (V_I) and diode junction voltage waveform (V_j) [11]

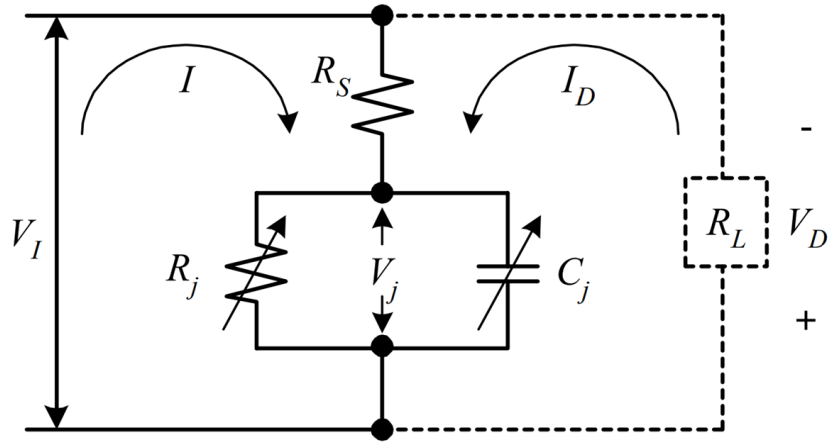

Figure 3.5: Equivalent circuit model of the half-wave rectifier [12]

The DC output voltage is determined from the rectified voltage across the diode junction V_j. Equation (3.11) is used to compute the average value of V_j in each cycle.

$$\begin{aligned} V_{j,dc} &= \frac{1}{2\pi}\int_{-\theta_{on}}^{\theta_{on}} V_{bi}\ d\theta + \frac{1}{2\pi}\int_{\theta_{on}}^{2\pi-\theta_{on}} (-V_{j0} + V_{j1}\ cos\theta)\ d\theta \\ &= \frac{V_{bi}\theta_{on}}{\pi} - \frac{V_{j0}}{\pi}(\pi - \theta_{on}) + \frac{V_{j1}}{2\pi}(-2sin(\theta_{on})) \\ &= \frac{\theta_{on}}{\pi}V_{bi} - V_{j0}(1 - \frac{\theta_{on}}{\pi}) - \frac{V_{j1}}{\pi}sin(\theta_{on}) \end{aligned} \tag{3.11}$$

If the diode is switched on then $V_j = V_{bi}$ and from (3.8) we have

$$V_{bi} = -V_{j0} + V_{j1}cos\theta_{on} \tag{3.12}$$

When the diode is off, R_j is infinite and Kirchhoff's voltage law can be applied to the left side of the loop to get

$$-V_I + IR_S + V_j = 0 \tag{3.13}$$

with

$$I = \frac{d}{dt} C_j V_j \tag{3.14}$$

Equations (3.13) and (3.14) are combined to get

$$\frac{d}{dt}(C_j V_j) = \frac{(V_I - V_j)}{R_S} \tag{3.15}$$

where C_j can be expressed as a harmonic function of V_D

$$C_j = C_0 + C_1 cos(\omega t - \phi) + C_2 cos(2\omega t - 2\phi) + ... \tag{3.16}$$

Combining only the DC and fundamental frequency components of (3.16) with (3.15), (3.8) and (3.7) yields

$$\begin{aligned} \omega R_S \ (C_1 V_{j0} - C_0 V_{j1}) sin \ \theta = V_{j0} - V_D + (V_P \ cos \ \phi - V_{j1}) \ cos \ \theta \\ - V_P sin \ \phi \ sin \ \theta \end{aligned} \tag{3.17}$$

where, for brevity, the substitution $\theta = \omega t - \phi$ is made. Collecting similar terms results in

$$V_{j0} = V_D \tag{3.18}$$

$$V_{j1} = V_P cos \ \phi \tag{3.19}$$

$$V_P \ sin \ \phi = \omega R_S (C_1 V_{j0} - C_0 V_{j1}) \tag{3.20}$$

Substituting (3.18) to (3.11) and inserting (3.11) into (3.10) gives

$$\frac{R_S}{R_L} = \frac{V_{j1}}{\pi V_D} \ sin \ \theta_{on} - \frac{\theta_{on}}{\pi} \ (1 + \frac{V_{bi}}{V_D}) \tag{3.21}$$

Ignoring the phase difference between V_I and V_j results in $V_P = V_{j1}$. Inserting

this and (3.18) into (3.12) and (3.21) obtains the most important relationship in determining the efficiency of the diode:

$$tan\ (\theta_{on}) - \theta_{on} = \frac{\pi R_S}{R_L(1 + \frac{V_{bi}}{V_D})} \tag{3.22}$$

Equation (3.22) is a transcendental expression that allows us to find the turn on angle of the diode θ_{on} iteratively. Once θ_{on} is solved for any given V_D, R_S and R_L, the efficiency and input impedance can be calculated from the time domain waveform V_I and V_j.

The overall diode efficiency can be expressed as

$$\eta_D = \frac{P_{dc}}{P_L + P_{dc}} \tag{3.23}$$

where V_o is the output voltage, P_L is the power dissipated by the diode (diode loss) and P_{dc} is the DC output power across the load, R_L. P_{dc} and P_L are given by

$$P_{dc} = \frac{V_o^2}{R_L} \tag{3.24}$$

$$P_L = L_{on,R_S} + L_{off,R_S} + L_{on,diode} \tag{3.25}$$

where L_{on,R_S} and L_{off,R_S} represent the power lost due to the series parasitic resistance when the diode is forward or reverse biased; $L_{on,diode}$ is the power lost due to the diode junction when the diode is forward biased. Note the loss through the diode junction when the diode is turned off has been neglected since it is assumed the junction resistance is infinite in that operation. These losses are the time average products of the current flowing through an ele-

ment and the voltage across that element, which will be important in defining the input impedance of the diode later. L_{on,R_S}, L_{off,R_S} and $L_{on,diode}$ can be expressed by

$$L_{on,R_S} = \frac{1}{2\pi} \int_{-\theta_{on}}^{\theta_{on}} \frac{(V_I - V_{bi})^2}{R_S} \, d\theta \tag{3.26}$$

$$L_{off,R_S} = \frac{1}{2\pi} \int_{\theta_{on}}^{2\pi-\theta_{on}} \frac{(V_I - V_D)^2}{R_S} \, d\theta \tag{3.27}$$

$$L_{on,diode} = \frac{1}{2\pi} \int_{-\theta_{on}}^{\theta_{on}} \frac{(V_I - V_{bi})V_{bi}}{R_S} \, d\theta \tag{3.28}$$

The total power dissipated by the series resistance can be solved by integrating

$$L_{R_S} = \frac{1}{2\pi R_S} \left[\int_{-\theta_{on}}^{\theta_{on}} (-V_D - V_{bi} + V_P \, cos \, \theta)^2 \, d\theta + (\omega R_S C_j V_P)^2 \int_{\theta_{on}}^{2\pi-\theta_{on}} sin^2\theta \, d\theta \right] \tag{3.29}$$

Using current instead of voltage, the equation for the loss in the series resistance when the diode is off (3.27) is rewritten:

$$L_{off,R_S} = \frac{1}{2\pi} \int_{\theta_{on}}^{2\pi-\theta_{on}} \frac{(V_I - V_j)^2}{R_S} \, d\theta = \frac{1}{2\pi} \int_{\theta_{on}}^{2\pi-\theta_{on}} \frac{(IR_S)^2}{R_S} \, d\theta \tag{3.30}$$

where I is the RF current flowing through the diode in reverse bias. It is assumed no current flows through R_j in reverse bias and all the current that flows through R_S also flows through the capacitor C_j. Thus, (3.14) can be rewritten as

$$I = C_j \frac{dV_j}{dt}. \tag{3.31}$$

We assume the voltage drop across R_S is small enough during the off cycle that the phase difference ϕ is set to zero. Making $\phi = 0$ in (3.21) gives $V_{j1} = V_P$.

Now

$$I = C_j \frac{d}{dt} \left[-V_{j0} + V_P \; cos(\omega t) \right] = -\omega C_j V_P \; sin \; \theta. \tag{3.32}$$

The loss in the diode junction becomes a combination of (3.28) and (3.7) as

$$L_{diode} = \frac{1}{2\pi R_S} \int_{-\theta_{on}}^{\theta_{on}} V_{bi}(-V_D - V_{bi} + V_P \; cos \; \theta) \; d\theta \tag{3.33}$$

where V_P can be determined during the off cycle of the diode by

$$V_P = \frac{V_D + V_{bi}}{cos \; \theta_{on}}. \tag{3.34}$$

Solutions to the integrals in (3.29) and (3.33) are plugged into (3.23) to yield

$$\eta_D = \frac{1}{1 + A + B + C} \tag{3.35}$$

where

$$A = \frac{R_L}{\pi R_S} \left(1 + \frac{V_{bi}}{V_D} \right)^2 \left[\theta_{on} \left(1 + \frac{1}{2 \cos^2 \; \theta_{on}} \right) - \frac{3}{2} \tan \; \theta_{on} \right] \tag{3.36}$$

$$B = \frac{R_S R_L C_j^2 \omega^2}{2\pi} \left(1 + \frac{V_{bi}}{V_D} \right) \left(\frac{\pi - \theta_{on}}{\cos^2 \; \theta_{on}} + \tan \; \theta_{on} \right) \tag{3.37}$$

$$C = \frac{R_L}{\pi R_S} \left(1 + \frac{V_{bi}}{V_D} \right) \frac{V_{bi}}{V_D} \left(\tan \; \theta_{on} - \theta_{on} \right) \tag{3.38}$$

with $\omega = 2\pi f$. The diode junction capacitance is given by

$$C_j = C_{j0} \sqrt{\frac{V_{bi}}{V_{bi} + |V_D|}} \tag{3.39}$$

where C_{j0} is the zero bias junction capacitance of the diode. Equations (3.35)-(3.39) can be used to solve for the diode's overall efficiency.

The input impedance of the diode can be solved for from the current I flowing through R_S in one cycle, or

$$I = I_0 + I_{1r}\cos\omega t + I_{1i}\sin(\omega t) \tag{3.40}$$

where I_0 is the DC component; I_{1r} and I_{1i} are the real and imaginary parts of the fundamental frequency component. In [12], these current components are solved by the following integrals

$$I_0 = \frac{1}{2\pi R_S}\left[\int_{-\theta_{on}}^{\theta_{on}}(V_I - V_{bi})\ d\theta + \int_{\theta_{on}}^{2\pi-\theta_{on}}(V_I - V_j)\ d\theta\right] \tag{3.41}$$

$$I_{1r} = \frac{1}{\pi R_S}\left[\int_{-\theta_{on}}^{\theta_{on}}(V_I - V_{bi})\cos(\theta+\phi)\ d\theta + \int_{\theta_{on}}^{2\pi-\theta_{on}}(V_I - V_j)\cos(\theta+\phi)\ d\theta\right] \tag{3.42}$$

$$I_{1i} = -\frac{1}{\pi R_S}\left[\int_{-\theta_{on}}^{\theta_{on}}(V_I - V_{bi})\sin(\theta+\phi)\ d\theta + \int_{\theta_{on}}^{2\pi-\theta_{on}}(V_I - V_j)\sin(\theta+\phi)\ d\theta\right]. \tag{3.43}$$

Now the diode input impedance can be defined at the fundamental frequency of operation as

$$Z_D = \frac{V_P}{I_{1r} - jI_{1i}}. \tag{3.44}$$

If it is assumed that during forward bias there is no current flowing through C_j and that all current is flowing through during reverse bias, then the diode current in one cycle can be found by integrating

$$\begin{aligned} I_{1r} - jI_{1i} = \frac{1}{\pi R_S}\int_{-\theta_{on}}^{\theta_{on}}(-V_D - V_{bi} + V_P\cos\theta)\cos\theta\ d\theta\ + \\ j\frac{\omega C_j V_P}{\pi}\int_{\theta_{on}}^{2\pi-\theta_{on}}\sin^2\theta\ d\theta. \end{aligned} \tag{3.45}$$

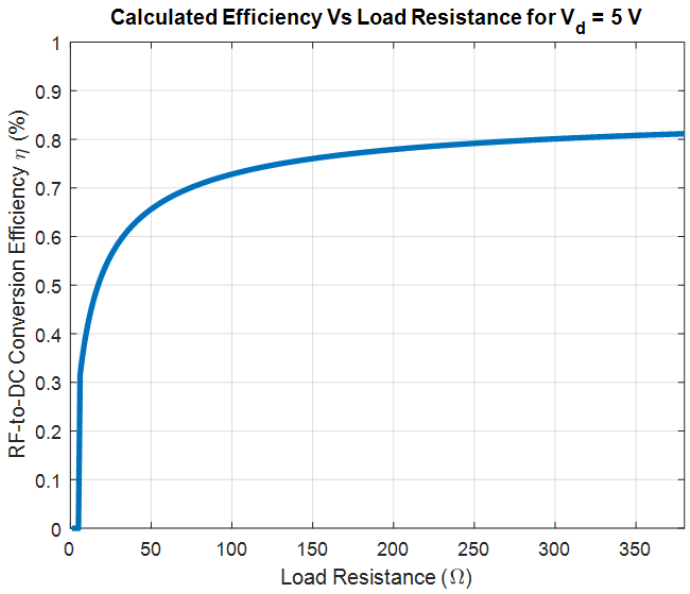

Figure 3.6: Diode Efficiency as a Function of Load Resistance

The diode input impedance can then be defined as

$$Z_D = \frac{\pi R_S}{\cos\theta_{on}\left(\frac{\theta_{on}}{\cos\theta_{on}} - \sin\theta_{on}\right) + j\omega R_S C_j\left(\frac{\pi-\theta_{on}}{\cos\theta_{on}} + \sin\theta_{on}\right)} \tag{3.46}$$

In the rectenna design, a capacitor is placed away from the diode in order to tune out the reactance of the diode, making the diode's input impedance

$$R_D = \frac{\pi R_S}{\cos\theta_{on}\left(\frac{\theta_{on}}{\cos\theta_{on}} - \sin\theta_{on}\right)} \tag{3.47}$$

The diode used in this work is the MACOM MA4E1317. The diode parameters can be found in Table 3.1. In choosing a load resistor, the trend of Figure 3.6 was considered. The plot shows the efficiency values leveling out around the 200 Ω point so a resistor equal or greater than 200 Ω should be chosen. When considering Figures 3.7 we see that as we choose a larger load resistance, the reactance of the diode input impedance gets more capacitive,

and the resistance grows larger. As these values become larger, there is intrinsically more loss through the diode. A good resistance value of $R_L = 250\ \Omega$ was eventually chosen for use in the rectenna. For this resistor at 10 GHz, the diode input impedance was found to be $Z_D = 171.89 - j\ 16.9\ \Omega$ with $V_D = V_B/2 = 3.5\ V$. The diode should be pushed to its voltage maximums to ensure the reactive component of the input impedance is minimized. The authors of [13] note the MA4E1317 has been shown to produce output voltages up to 5 V. Setting $V_D = 5\ V$ with a load resistor of $R_L = 250\ \Omega$ makes the input impedance to the diode $Z_D = 164.61 - j\ 13.3\ \Omega$. Figure 3.8 shows a plot of the real and complex parts of the diode impedance as a function of R_L for $V_D = 5\ V$. Figure 3.9 shows the affects the diode voltage has on the input impedance. Figures 3.10 and 3.11 show the efficiency of the diode as a function of power and voltage, respectively, using equation (3.35).

Table 3.1: MACOM MA4E1317

Parameter	Symbol	Units	Value
Junction Capacitance	C_j	pF	0.02
Series Resistance	R_S	Ω	4
Turn-On/Bias Voltage	V_{bi}	V	0.7
Breakdown Voltage	V_B	V	7

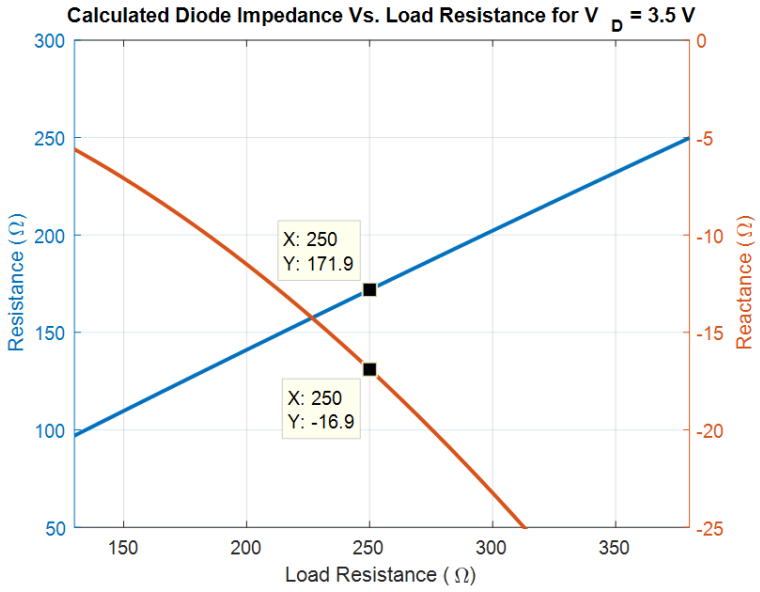

Figure 3.7: Calculated Diode Impedance vs Load Resistance at $f = 10\ GHz$ and $V_D = 3.5\ V$

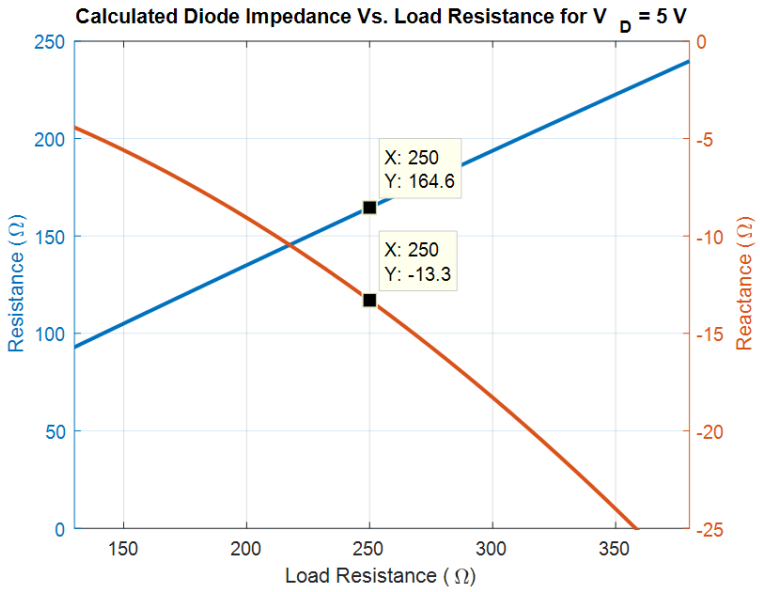

Figure 3.8: Calculated Diode Impedance vs Load Resistance at $f = 10\ GHz$ and $V_D = 5\ V$

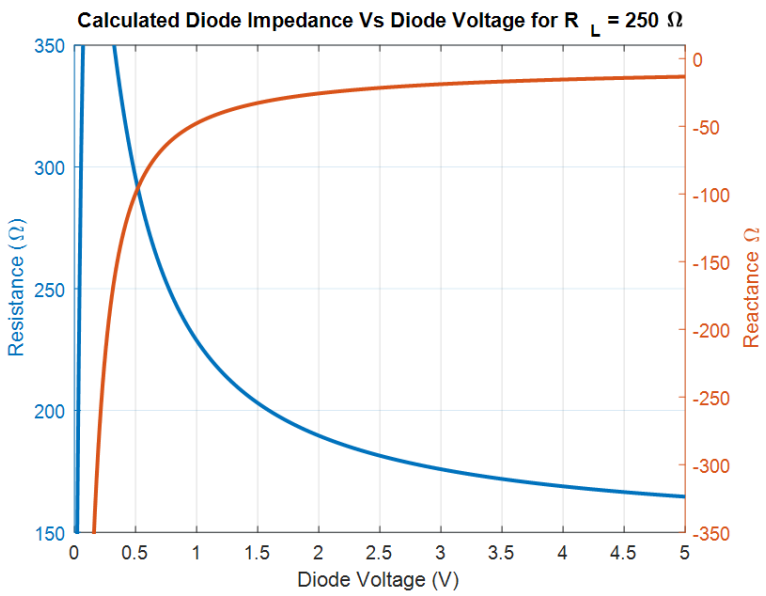

Figure 3.9: Calculated Diode Impedance vs Diode Voltage for a 250 Ω Load Resistance

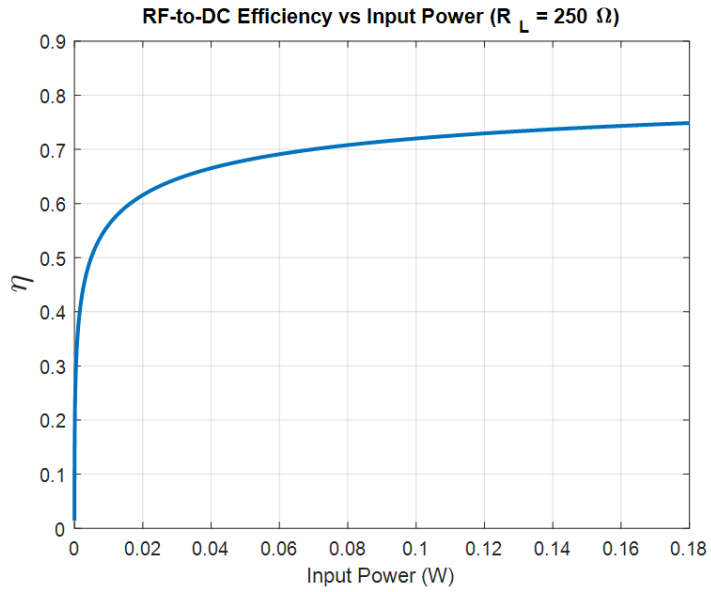

Figure 3.10: Diode Efficiency vs Input Power for a 250Ω Load Resistance

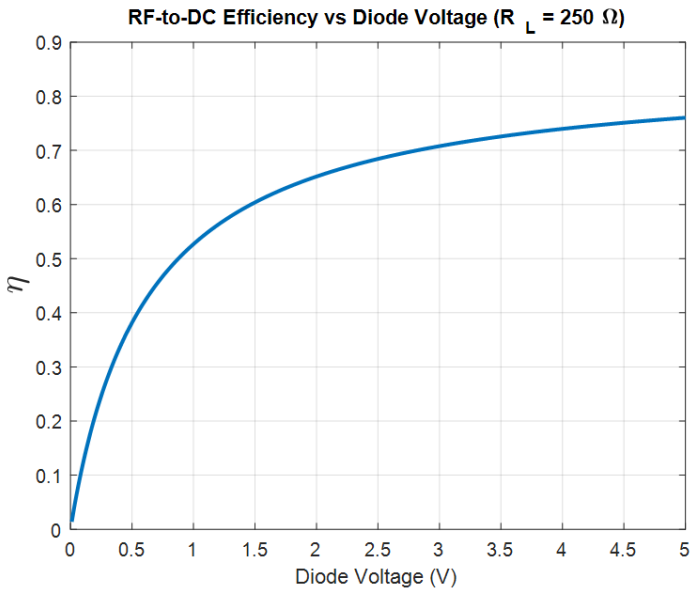

Figure 3.11: Diode Efficiency vs Diode Voltage for a 250Ω Load Resistance

Chapter 4

Rectenna Single Element Design

4.1 The Coplanar Strips Transmission Line

In choosing a transmission line for the rectenna structure, several things must be kept in mind: first, the transmission line must have a relatively high characteristic impedance in order to match to the diode's input impedance of $171.89 - j16.9\ \Omega$; second, it should allow for the implementation of surface mount components; third, it must allow for compact filter implementations; fourth the transmission line must be inherently low loss. The coplanar strip transmission line, or coplanar stripline (CPS), can satisfy all of these requirements.

CPS is a differentially fed transmission line that exists as two strips of conductor sitting on top of a substrate. It is easy to think about as the inverse of the coplanar waveguide (CPW) transmission line. While CPW has been studied at great length, CPS has been relatively neglected. However, CPS is superior to CPW in that it allows easy shunt and series mounting of active and passsive devices and it eliminates the need for via holes which introduce additional parasitic elements, while maintaining the low profile and efficient use of space advantages of CPW. There are several types of CPS: symmetric

CPS where the widths of the two conductors are the same and lie on the same layer of the substrate; asymmetric CPS where the conductors can be of different widths and exist on different layers of the substrate, and ground-backed CPS as well. The dual-rhombic loop antenna (DRLA) being used for this rectenna requires symmetric CPS in order for both loops to exist on the top layer of the substrate, and a reflecting plane to exist behind the structure.

Analytic techniques for calculating the characteristics of CPS have been developed in [19]. The calculated relative permittivity of CPS can be found from

$$\epsilon_{eff} = 1 + \frac{\epsilon_r - 1}{2} \frac{K(k_1')}{K(k_1)} \frac{K(k_2)}{K(k_2')} \left[\frac{Farad}{unit\ length} \right] \tag{4.1}$$

where ϵ_r is the substrate's dielectric constant and K and K' represent elliptic integrals of the first kind. The values of k_1 and k_2 can be solved for using

$$k_1 = \frac{s}{s + 2W} = \frac{a}{b} \tag{4.2}$$

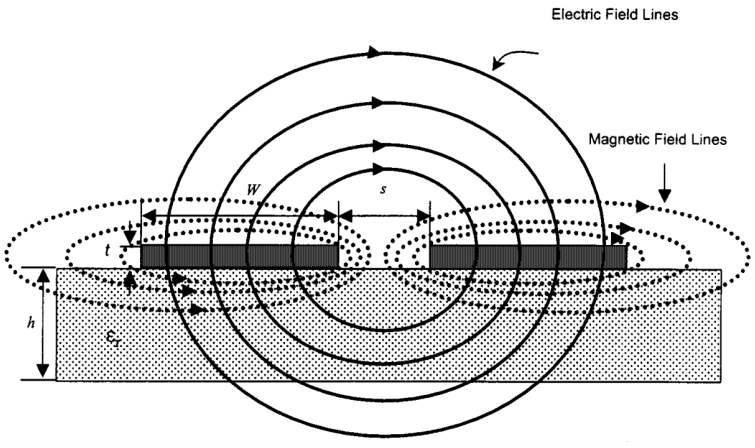

Figure 4.1: Coplanar Stripline Structure [18]

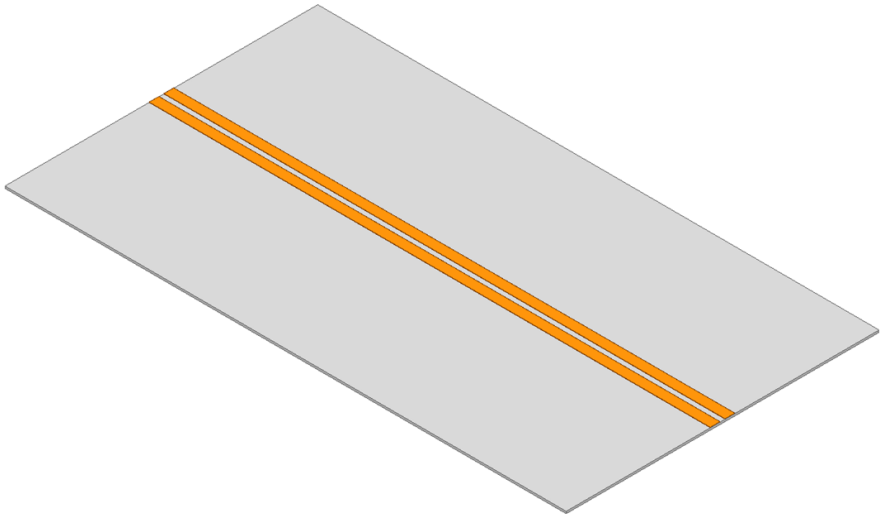

Figure 4.2: CPS Thru Modeled in HFSS

$$k_2 = \frac{\sinh\frac{\pi a}{2h}}{\sinh\frac{\pi b}{2h}} \tag{4.3}$$

$$a = \frac{s}{2} \qquad b = \frac{s}{2} + W \qquad k' = \sqrt{1-k^2} \tag{4.4}$$

and the characteristic impedance Z_o is calculated using

$$Z_o = \frac{120\pi}{\sqrt{\frac{\epsilon_{eff}+1}{2}}\frac{\pi}{ln\left(2\,\frac{1+(1-k_1^2)^{\frac{1}{4}}}{1-(1-k_1^2)^{\frac{1}{4}}}\right)}}. \tag{4.5}$$

It is also interesting in this research to consider the attenuation as a function of the characteristic impedance. For coplanar stripline, the conductor attenuation α_c and dielectric attenuation α_d is calculated as follows

$$\alpha_c = \frac{8.68R_s\sqrt{\epsilon_{eff}}}{480\pi K(k_1)K(k_1')(1-k_1^2))} \times \left[\frac{1}{a}\left[\pi + ln(\frac{8\pi a(1-k_1)}{t(1+k_1)})\right] + \frac{1}{b}\left[\pi + ln(\frac{8\pi b}{t}\frac{1-k_1}{1+k_1})\right]\right] \tag{4.6}$$

$$\alpha_d = 27.3 \frac{\epsilon_r}{\sqrt{\epsilon_{eff}}} \frac{\epsilon_{eff} - 1}{\epsilon_r - 1} \frac{\tan \delta}{\lambda_0} \tag{4.7}$$

where R_s is the surface resistance in ohms and δ is the skin depth. Figure 4.3 shows equations (4.6) and (4.7) as a function of the separation width of the CPS line. It is very convenient that, for CPS, as the characteristic impedance gets larger, the attenuation per unit length gets smaller.

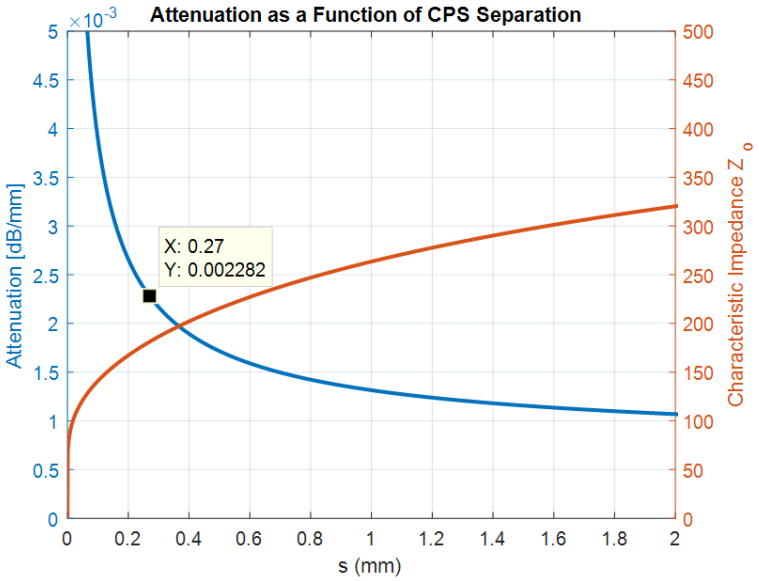

Figure 4.3: Coplanar Stripline Attenuation (α_c+α_d) as a function of separation width (s) at 10 GHz, W = 0.47 mm, h = 0.1 mm and $\epsilon_r = 2.5$

ANSYS HFSS was used to simulate the CPS structure and extract ϵ_{eff} and Z_0. For comparison, equations (4.1) and (4.5) were computed in MATLAB setting $W = 0.47\ mm$, $f = 10\ GHz$, $h = 0.1\ mm$, and $s = 0.27\ mm$ which were the final values used in the actual design. The results are seen in Table 4.1 as well as Figure 4.4 and Figure 4.5. Where guided wavelength, λ_g is found by solving

$$\lambda_g = \frac{c}{f\sqrt{\epsilon_{eff}}}. \tag{4.8}$$

Table 4.1: CPS MATLAB vs HFSS Comparison

Parameter	MATLAB	HFSS
Characteristic Impedance (Z_0)	177.09 Ω	172.42 Ω
Effective Permittivity (ϵ_{eff})	1.2042	1.3058
Free space Wavelength (λ_0)	30 mm	30 mm
Guided Wavelength (λ_g)	27.34 mm	26.25 mm

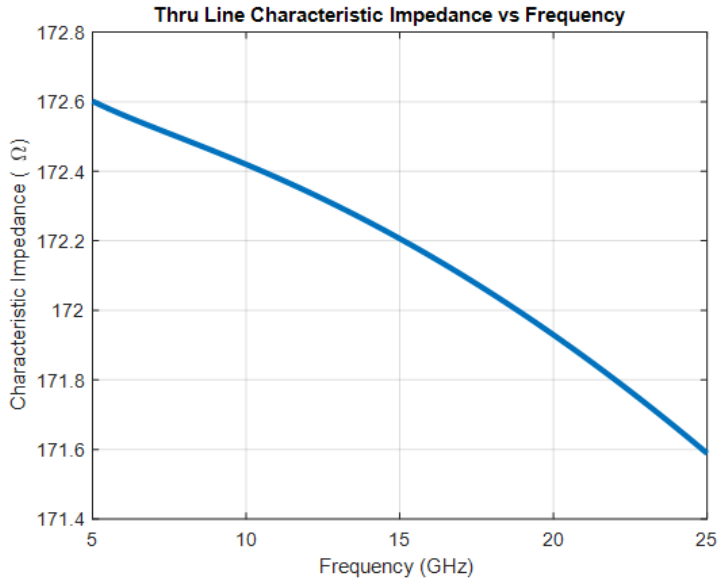

Figure 4.4: Plot of Z_0 vs Frequency for the HFSS Thru Line Model

4.2 The Dual Rhombic Loop Antenna

For space-to-terrestrial or terrestrial-to-space WPT systems, the design of the rectenna should seek to be a high gain, circularly polarized antenna so as to allow the antenna to be rotated without changing the output voltage. Circularly polarized antennas also have the advantage of disregarding the effects of the ionosphere on electromagnetic wave propagation in the case of space-to-terrestrial power transfer. Previous research in rectenna design has shown the feasibility of antennas such as the printed dipole [20] by Raytheon Company, a slotline-fed slot antenna [21], a circularly polarized patch antenna [22], cir-

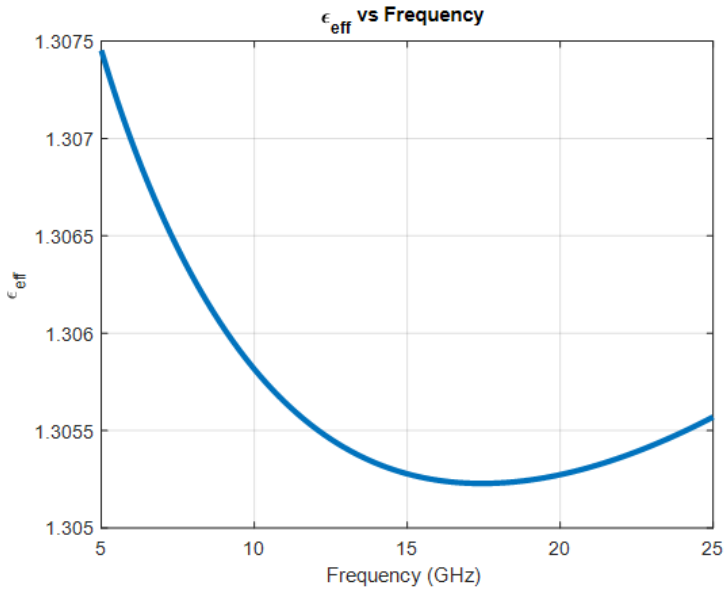

Figure 4.5: HFSS Model of CPS for ϵ_{eff}

cularly polarized spiral antennas [23] and a circularly polarized dual rhombic loop antenna [13]. The dual rhombic loop antenna was chosen for this project as it can provide circular polarization as well as relatively high gain when compared with the truncated patch and spiral antenna designs. The use of a high gain antenna has the advantage of reducing the number of rectenna elements in an array that are necessary to cover the same receiving area - since the effective aperture of an antenna is proportional to it's gain.

The dual rhombic loop antenna consists of two rhombic loop antennas, both of the same size, that exist above a reflecting plane. The reflecting plane is used to enhance the gain in the broadside direction. Both loops have a gap located symmetrically across from one another in order to induce left hand or right hand circular polarization (LHCP/RHCP). The sense of circular polarization can be easily switched from left-hand to right-hand by switching the gap positions.

The authors of [24] suggest the total perimeter of the loops should be equal

Table 4.2: DRLA Dimensions from [24] vs Simulated Values from HFSS

Dimension	Theoretical	HFSS
Perimeter ($4L$)	38.7 mm	44 mm
DRLA Width (W)	0.48 mm	0.48 mm
Center to Center Separation (C)	0.75 mm	0.75 mm
Location of Gap (S)	N/A	10.735 mm
Gap Size (ΔS)	N/A	2.9 mm
Reflecting Plane Distance	7.5 mm	9.7 mm

to approximately $1.29\lambda_0$ (4L in Figure 4.6), where λ_0 is calculated from the center operating frequency. The antenna induces a circularly polarized wave by generating a constant amplitude current density with a linearly changing phase. The width of each section (W) should be .016 λ_0 and a third suggestion is that the middle of the CPS feed lines should be separated by $.025\lambda_0$ determining the separation of the two rhombic loops (C). Finally, the reflecting plane should be placed $\lambda_0/4$ behind the antenna. The positioning of the gaps (as shown in Figure 4.6) generates the left-hand circular polarization and the axial ratio is very sensitive to the size and placement of these gaps.

The suggested values for the DRLA can be seen in Table 4.6 as well as the adjustments made over several iterations in ANSYS HFSS. All variables from Table 4.2 reference Figure 4.6. Using the values from Table 4.6 in the HFSS column, the resulting LHCP realized gain pattern is plotted in Figure 4.7. The designed DRLA exhibits 10.04 dB of LHCP realized gain. The input impedance at the antenna's terminals is 133.61 Ω as shown in Figure 4.8. Figure 4.9 shows the antenna has a good match at 10 GHz with a return loss of greater than 30 dB. Finally, as shown in Figure 4.10, the DRLA has an axial ratio of 1.96 dB, which is a figure of merit for circular polarization.

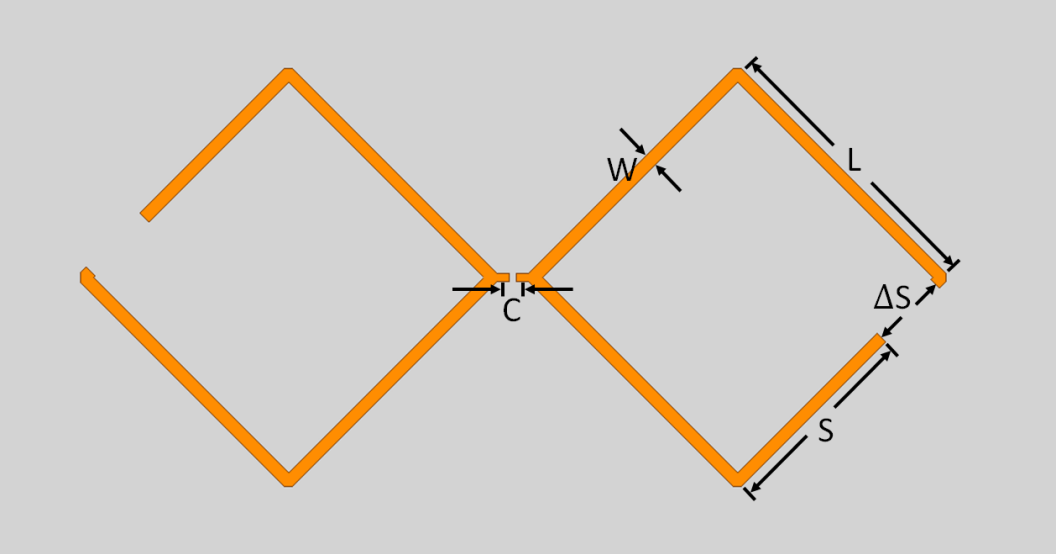

Figure 4.6: HFSS Model of DRLA

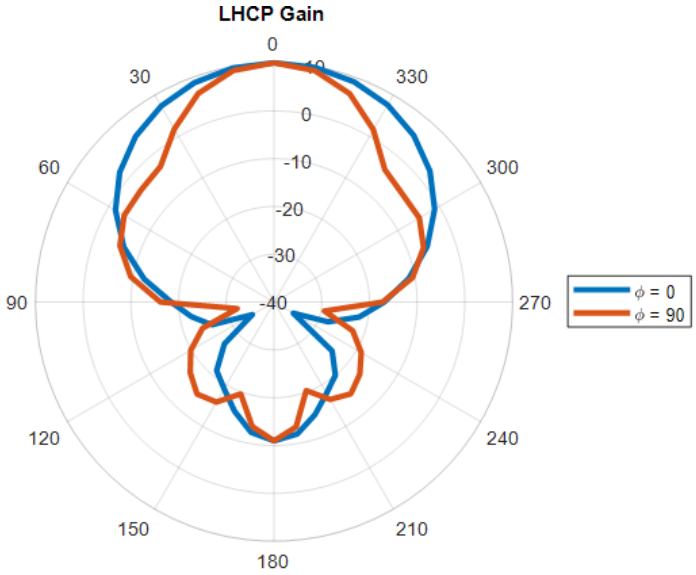

Figure 4.7: DRLA LHCP Realized Gain Simulated in HFSS

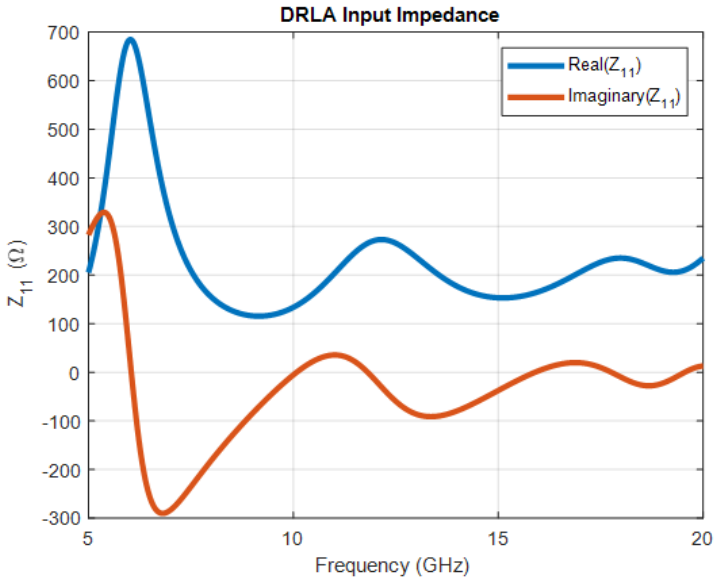

Figure 4.8: DRLA Input Real and Imaginary Input Impedance Simulated in HFSS

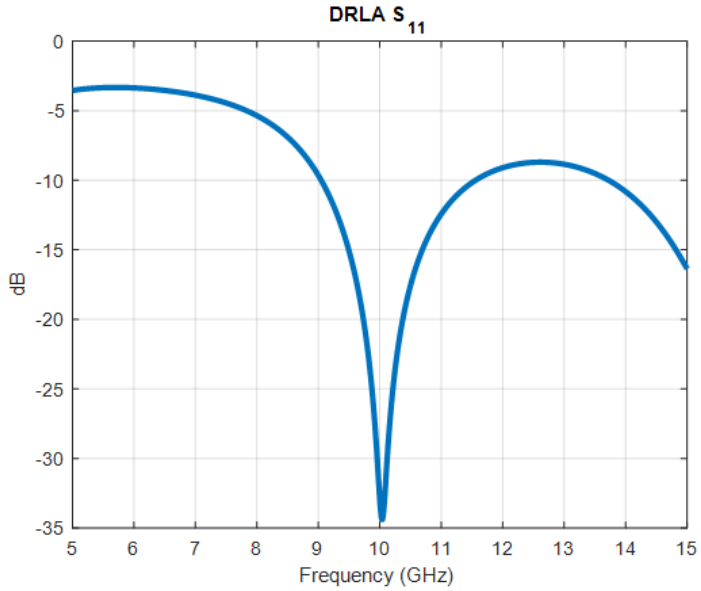

Figure 4.9: Simulated S_{11} for DRLA

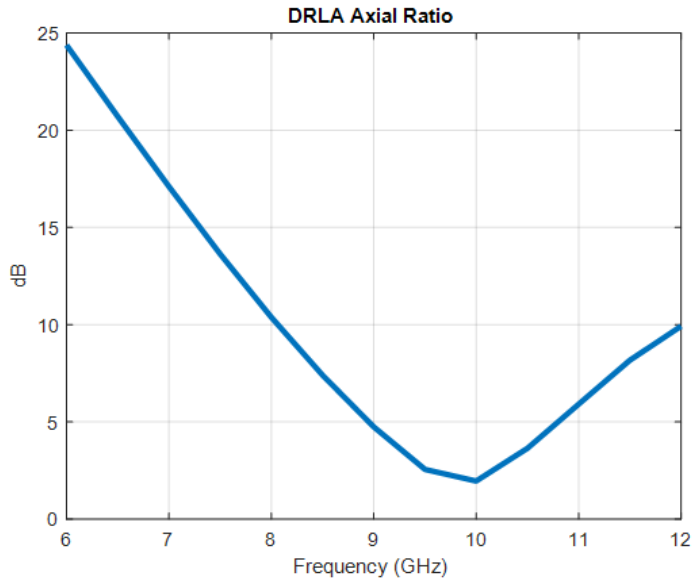

Figure 4.10: Simulated Axial Ratio for DRLA

4.3 CPS Lowpass Filter and Quarter Wave Transformer

A CPS lowpass filter (LPF) was designed to pass 10 GHz while rejecting the higher order harmonics generated by the diode. The design of the filter is relatively simple. The LPF uses spur slot discontinuities in the CPS line based off of [25] and [26]. The spur slot creates a resonant structure in each side of the conductive strips on the top layer of the CPS and the filter response behaves much like any resonant filter would. The length of each cutout should be $\lambda_g/4$ to set the cut off frequency (f_c), and the slots can be moved closer or further from one another to adjust the roll-off of the filter. The width, length and spacing are tuned to provide the best match at 10 GHz and the most rejection at 20 GHz.

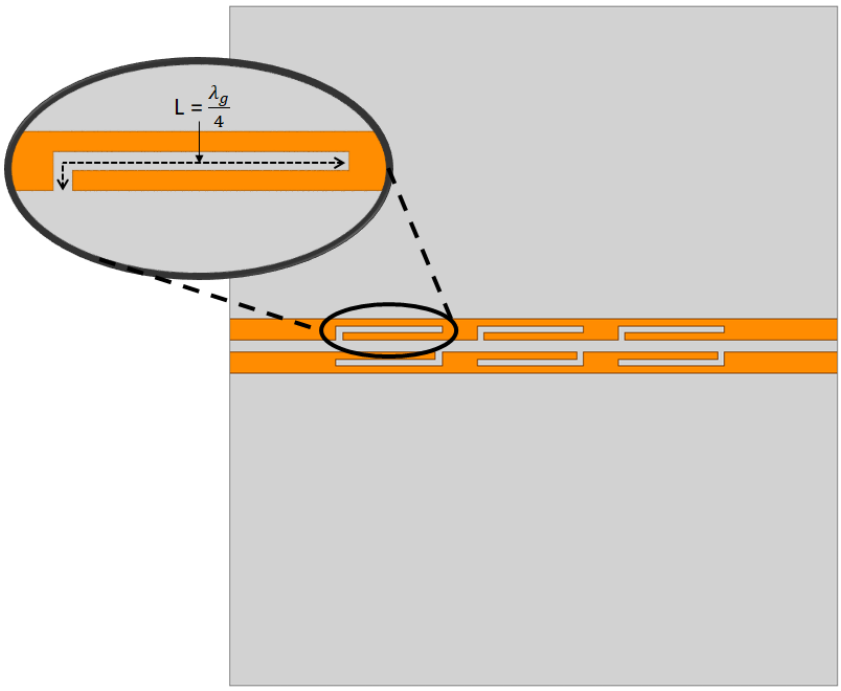

Figure 4.11: CPS Filter

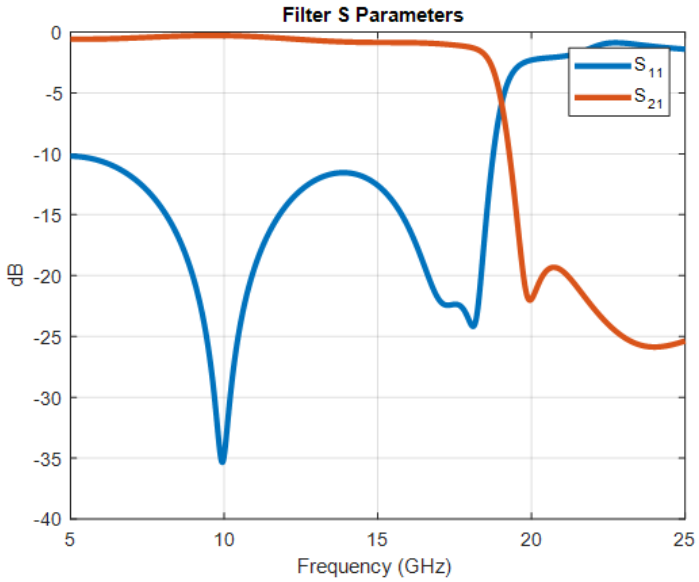

Figure 4.12: Simulated S-Parameters for the CPS Filter

The filter's simulated S-parameters from HFSS are shown in Figure 4.12. The simulation predicts an insertion loss of 0.28 dB and a return loss of 35.8 dB at 10 GHz while blocking 20 GHz from flowing by more than 21 dB. The filter is matched to 172 Ω at both ports to minimize reflections from the filter to the diode. In order for power to flow from the antenna to the diode, an impedance transformer will have to be implemented to match the 172 Ω input impedance of the filter (and thus the diode) to the 133.61 Ω input impedance of the antenna.

Since the rectenna is only really concerned with efficiently rectifying the 10 GHz signal while rejecting the 20 GHz signal, a narrow-band matching transformer will suffice. The simplest matching network to design and realize is the quarter-wave transformer. The characteristic impedance of the quarter-wave transformer is given as the geometric mean between the two impedances we want to match.

$$Z_{QW} = \sqrt{Z_{antenna} \cdot Z_{diode}} = 151.595\ \Omega \tag{4.9}$$

Using equations (4.1) and (4.5), the length, width and gap size of the quarter-wave section are solved for. The quarter wave transmission line has gap size of 0.188 mm, a width of 0.52 mm and a length of 4.648 mm. The quarter wave transformer is implemented between the antenna and the filter, and a thru line is used to move the filter away from the antenna so as not to adversely affect the radiation pattern. The cascaded antenna is seen in Figure 4.13 and its S-Parameter response in Figure 4.14. The cascade shows a good match at 10 GHz with 44 dB of return loss and an axial ratio of 1.35 dB. The antenna radiates LHCP with 9.5 dB of realized gain.

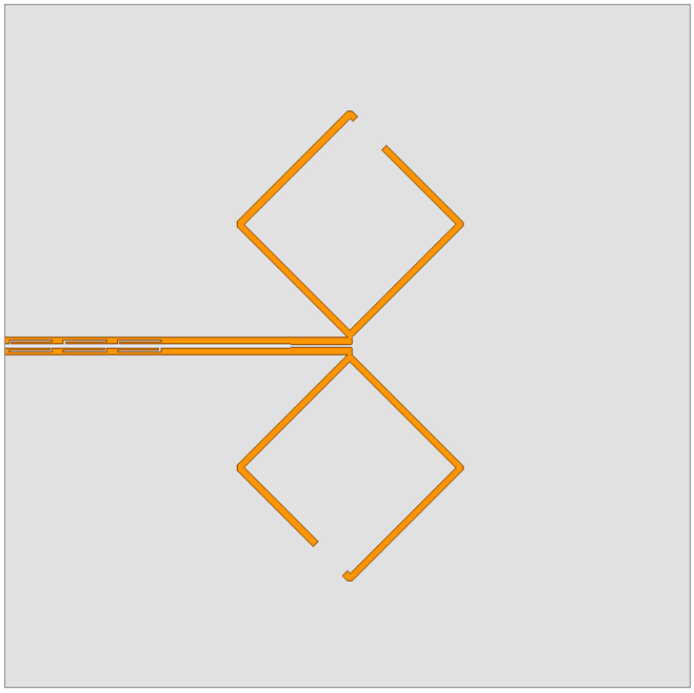

Figure 4.13: Cascaded DRLA with Filter

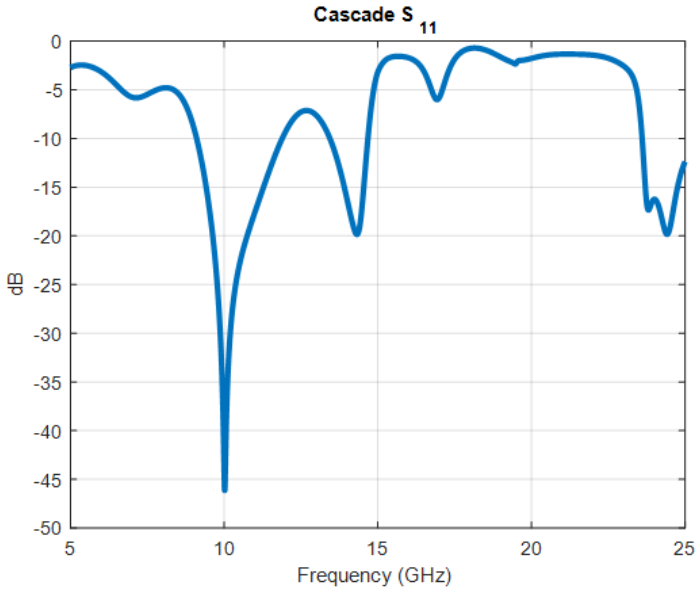

Figure 4.14: Cascade S_{11}

4.4 A Microstrip-to-CPS Balun

Before building the rectenna with the rectifier circuit, the antenna and filter cascade should first be characterized in an anechoic chamber. Since CPS is a balanced line, it is necessary to design and fabricate a microstrip-to-CPS balun. Several designs exist such as the balun in [27]; however, such baluns employ vias which significantly draw out the fabrication process. The balun used for this design is based off of [28] which can be easily fabricated using just a laser mill.

The electric field of CPS lines are formed across the two top conductors, but for microstrip, the field is orthogonal to the top trace. To rotate the electric field lines 90°, a radial stub is placed on one side at one end of the CPS line at an angle ϕ. This angle is optimized to be 30°relative to the CPS trace for strong coupling. On the bottom side of the substrate, the ground plane is smoothly tapered from underneath the radial stub, to just underneath one edge

of the microstrip. Since this design doesn't depend on the use of any quarter wavelength lines, bandwidth is preserved and the result is a very broadband microstrip-to-CPS balun.

In order to verify the design, back-to-back balun transitions were designed in HFSS matching the 50 Ω impedance of the microstrip line to the 172 Ω impedance of the CPS. Figure 4.15 shows the model with the orange patterning representing the top copper and the blue pattern representing the bottom. The microstrip line was tapered to the edge of the substrate in order to preserve the broadband response of the balun. The S-parameter response is seen in Figure 4.16.

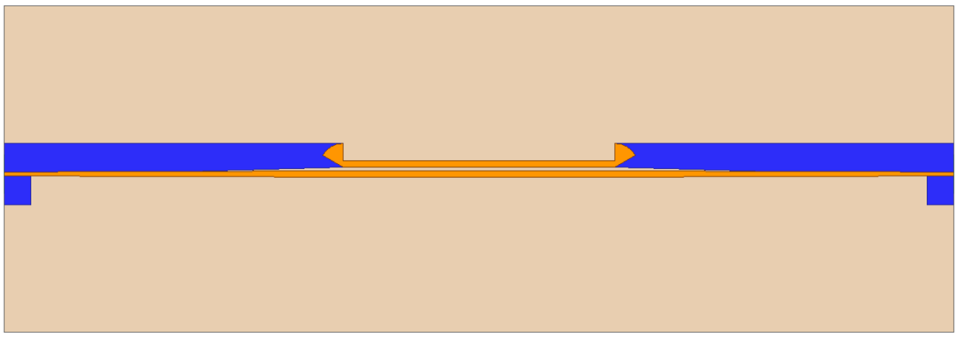

Figure 4.15: Back-to-Back Microstrip-to-CPS Balun Modeled in HFSS

4.5 DRLA+Filter+Balun

With the antenna, filter and balun all designed as individual components, the next step in developing the rectenna is to put these elements together in order

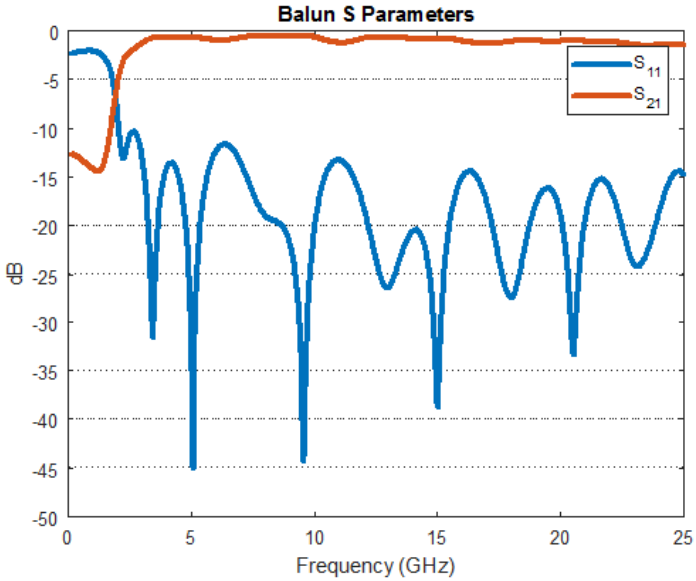

Figure 4.16: Back-to-Back Microstrip-to-CPS Balun Simulated S Parameters

to get a better idea of the qualitative characteristics of the rectenna. All components were designed to match to one another and steps were taken to ensure that physical dimensions would line up. In an effort to maintain the antenna's horizontal position over the reflecting plane, a mount was built for the Southwest Microwave edge launch connector. This was necessary because the flexible nature of the substrate becomes pulled down toward the reflecting plane by the heavy connector. If the antenna doesn't sit above the reflecting plane horizontally enough, there could be undesirable effects on the radiation pattern and return loss. The mount was designed in HFSS along with the CAD model for the connector. The file was then exported to a FormLabs Form 2 3D resin printer to be fabricated.

The simulated model used to obtain the return loss and gain patterns of the combined DRLA, filter and antenna is provided in Figure 4.17 and the corresponding fabricated element is pictured in Figure 4.18. The straight black lines pictured in the substrate are due to the hatching grid on the LPKF U4

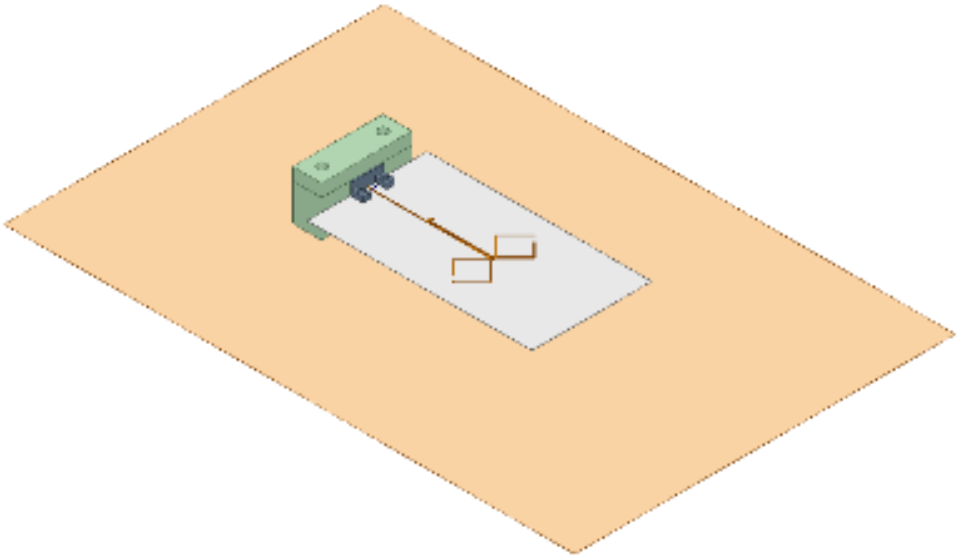

Figure 4.17: Simulation Model of DRLA+Filter+Balun

ProtoLaser laser mill not being set long enough and the mark speed for the pre-cut layer being set to slow. The lines are only slight cosmetic blemishes on the top and bottom layers of the substrate and should have little to no effect on the response of the antenna.

The cascaded elements were taken to the network analyzer for return loss measurements. A photograph of the measurement setup showing the fabricated antenna connected to the network analyzer is seen in Figure 4.19. The measured vs. simulated return loss is shown in Figure 4.20.

At 10 GHz, the return loss is around 18 dB. The differences between the simulated and measured return losses can be attributed to the lack of a proper fixture to mount the antenna at the proper height above the reflecting plane. The discrepancies might also be a result of difficulties in keeping the thin substrate completely flat and perfectly parallel to the reflecting plane. The nylon

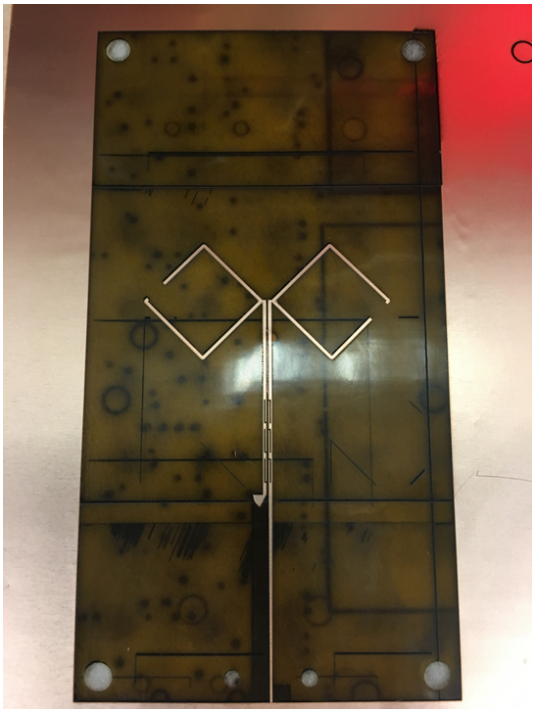

Figure 4.18: Rectenna with balun before being cut from substrate

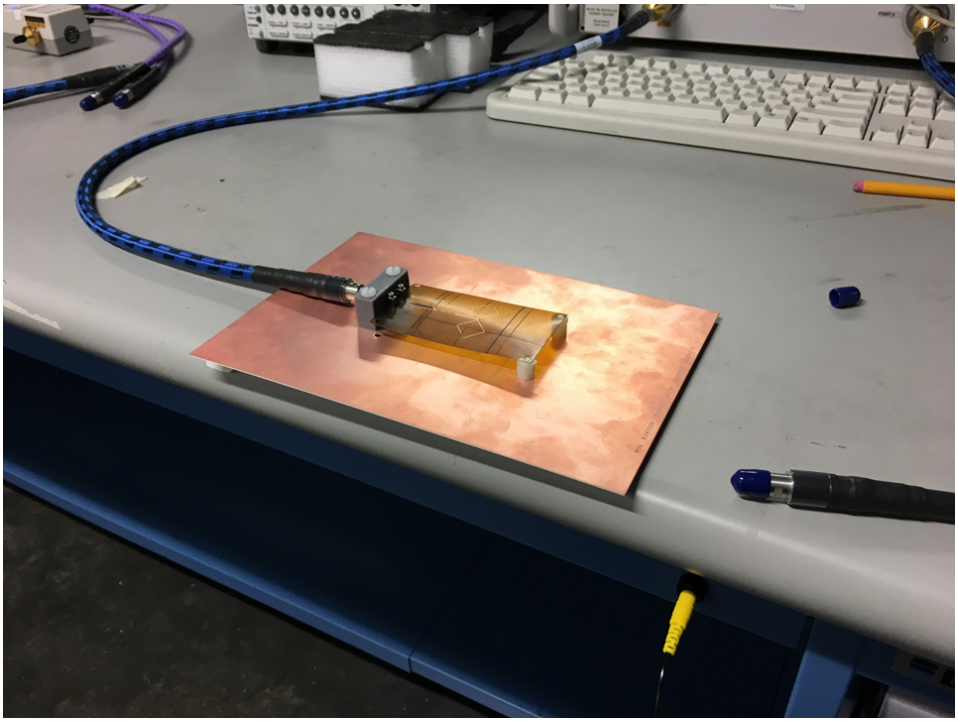

Figure 4.19: Photograph of the antenna setup for return loss measurements

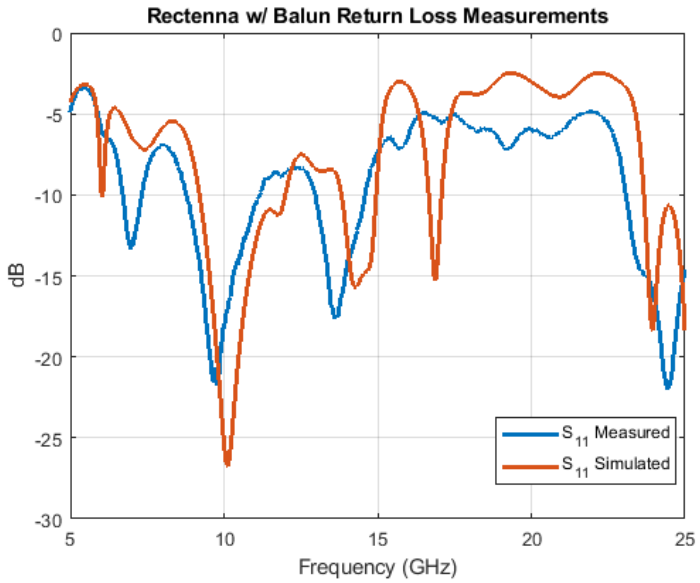

Figure 4.20: Measured vs. Simulated Return Loss

mounting screws that were used to mount the substrate above the reflecting plane were also not included in the simulation. Nonetheless, the shape of the measured return loss follows that of the simulation.

A mount was built for the antenna to be setup in the anechoic chamber for radiation pattern measurements. Figure 4.21 shows the antenna mounted in the chamber. Figures 4.22-4.23 show the normalized radiation patterns for E_θ and E_ϕ cuts and 4.24 shows the left hand circularly polarized gain plot that is not normalized. Overall, the measured patterns match the simulated very well, with very slight differences which may have been the result of alignment between transmit and receive antenna, as well as the aperture of the antenna not being perfectly centered above the reflecting plane. The realized gain plot does fall about 2.25 dB short of simulated. There are several reasons why this may be the case. The most likely is the reflecting plane distance was not accurately realized due to the nonrigid, narrow substrate. Another reason may be due to common mode currents not being effectively choked, causing

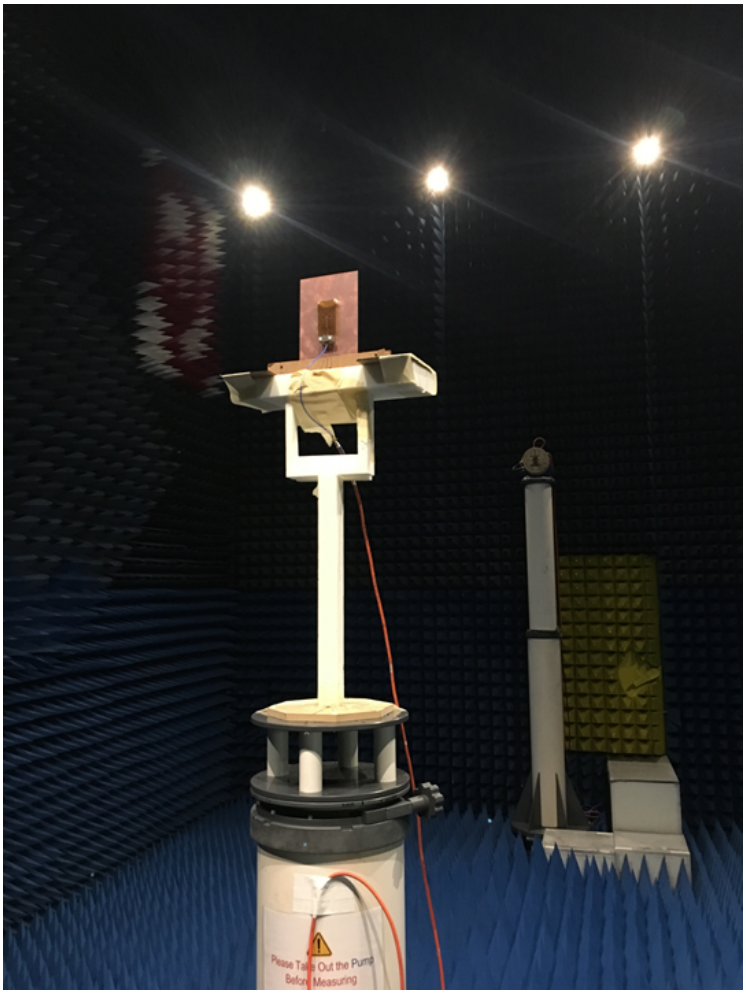

Figure 4.21: Photo of Rectenna in Anechoic Chamber

reflection currents on the cables which would take radiated power away from the antenna. A three port simulation was set up as seen in Figure 4.27 and the CMRR was solved for using

$$CMRR = 20 \cdot log\left(\frac{S_{21} + S_{31}}{S_{21} - S_{31}}\right). \tag{4.10}$$

The resulting plot can be seen in Figure 4.28. A CMRR of 24.6 dB at 10 GHz implies that the balun is choking the common mode currents.

Figure 4.25 shows the measured axial ratio of the antenna in dB as a

function of frequency. To find the axial ratio, equation (4.11) was used. The antenna has less than 3 dB axial ratio from 9 to 11 GHz showing it is definitely circularly polarized for the frequencies of interest.

$$AR = \frac{|E_\theta|}{|E_\phi|} \tag{4.11}$$

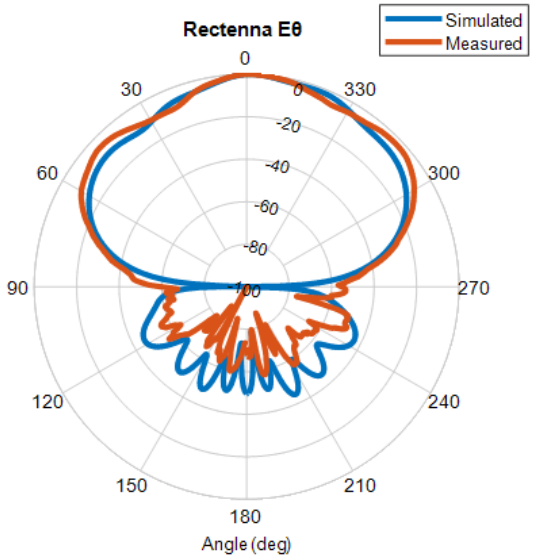

Figure 4.22: Rectenna Normalized Pattern for Theta Cut

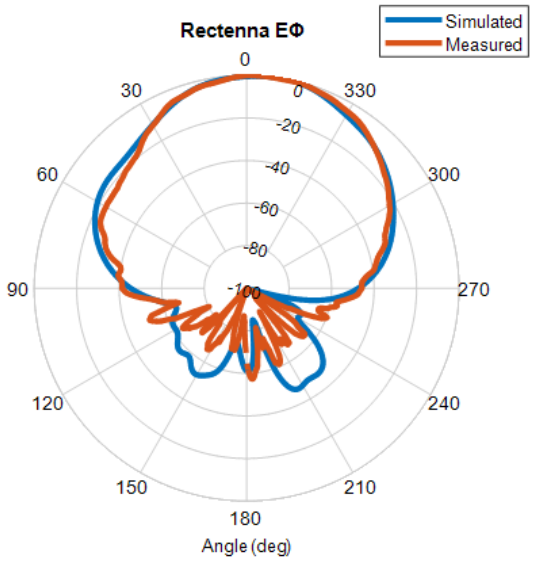

Figure 4.23: Rectenna Normalized Pattern for Phi Cut

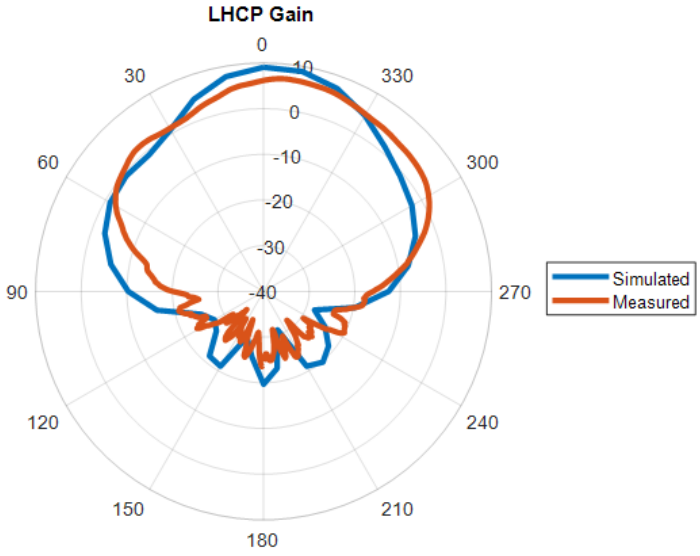

Figure 4.24: LHCP Gain Plot

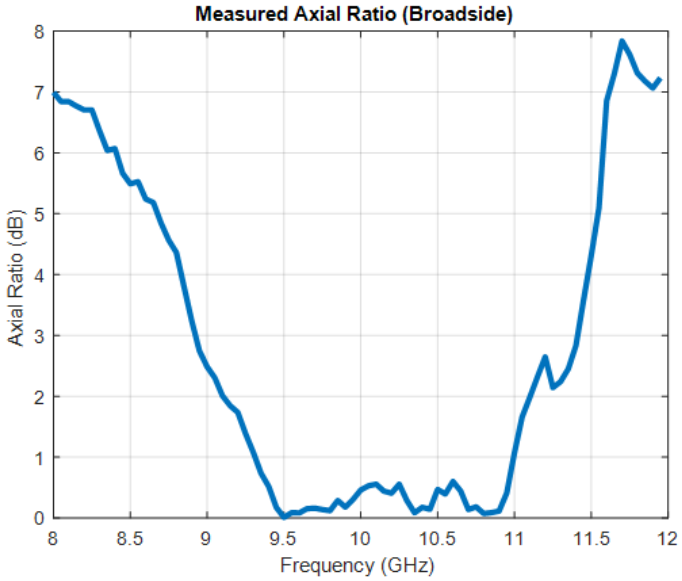

Figure 4.25: Measured Axial Ratio

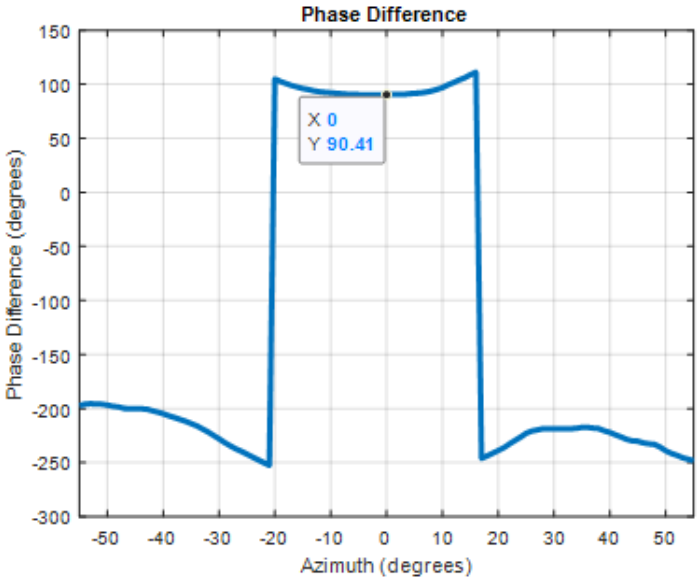

Figure 4.26: Phase Difference of 90°Indicating Circular Polarization

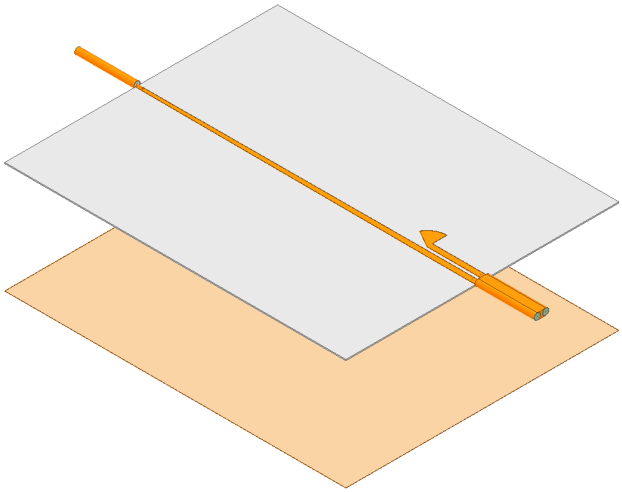

Figure 4.27: HFSS Model Used to Measure CMRR

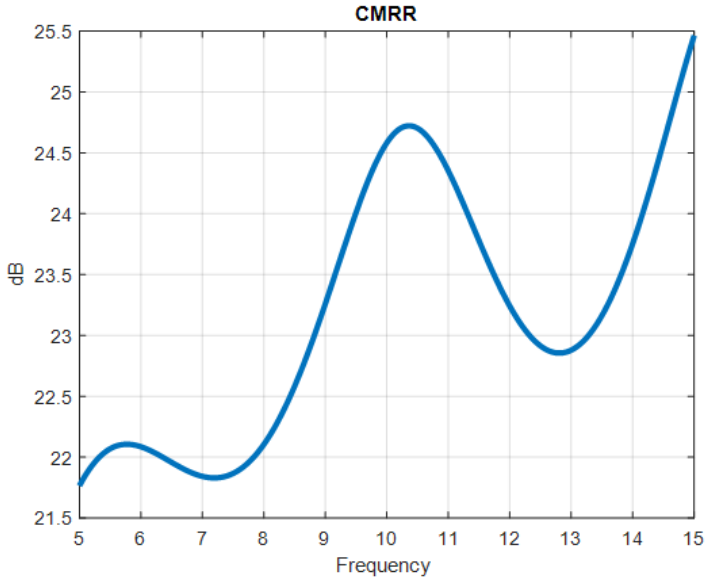

Figure 4.28: CMRR vs. Frequency

Chapter 5

Rectification and Efficiency

5.1 Results: RF-to-DC Efficiency

The diode used for RF-to-DC rectification is the MACOM flip chip detector diode MA4E1317. The diode parameters are found in Table 3.1. The diode, placed between the DC output capacitor and the low pass filter, will convert microwave energy into a large DC component at 10 GHz (fundamental frequency) and smaller DC components at its harmonics. The output capacitor used for the rectenna is the surface mount C08BL242X-5UN-X0 2.4 nF broadband blocking capacitor. The capacitor is rated to work from 1 MHz to 20 GHz. The resistive load is chosen to be 250 Ω. The resulting rectifier circuit's RC time constant is 600 nanoseconds, which is much greater than the period of a 10 GHz signal which is 0.1 nanoseconds.

The distance from the diode to the capacitor can have adverse effects on the output efficiency of the rectenna. The authors of [13] suggest the reactive component of the diode's input impedance should be tuned out to ensure maximum efficiency. The distance the authors used was $\lambda/4$. However, a somewhat more elegant approach to finding this length is used here.

The input impedance for the diode, solved from (3), is $Z_D = 171.89 - j\,16.9\,\Omega$

and the characteristic impedance of the CPS transmission line is 172.4 Ω. In order to tune out the reactance of the diode, a transmission line length that will make our input impedance to the load purely real is needed. Since the real part of the diode impedance is essentially matched to the real part of the CPS impedance (i.e. 171.89 Ω ≈ 172.4 Ω), the impedance of the diode lies directly underneath the matched point on the Smith chart (Point 1 in Figure 5.1). In order to shift the impedance to the real line (to point 2 in Figure 5.1) a transmission line of length $\lambda/8$ is needed. However, $\lambda/8$ represents a length that is approximately 3 mm - a very difficult length to realize when the width of the capacitor being used is 1.4 mm. However, as length of transmission line is added, the impedance simply rotates around the Smith Chart in a constant VSWR circle. Thus any integer multiple of a quarter-wavelength plus one-eighth of a wavelength ($\lambda/8 + n * \lambda/4$) will transform the reactance of the input impedance to zero. This concept is illustrated in Figure 5.1. Point 1 represents the location of the impedance of the diode while points 2 and 3 represent the points where the reactance of the diode is canceled by the transmission line.

For the rectenna built in this work, pads were also added to simplify mounting the components to the very small 0.47 mm traces of the CPS. The effect of the pads will add some capacitance but that should be negligible, especially considering the inductance that will be added by soldering the components in place. The final HFSS model is seen in Figure 5.2 and Figure 5.3 shows a photo of the final rectenna with the diode, capacitor and resistor soldered on. Extra substrate was added to the right side of the antenna in an attempt to better place the center of the DRLA aperture in the middle of the substrate, and later the reflecting plane, to minimize any possibilities of diffraction.

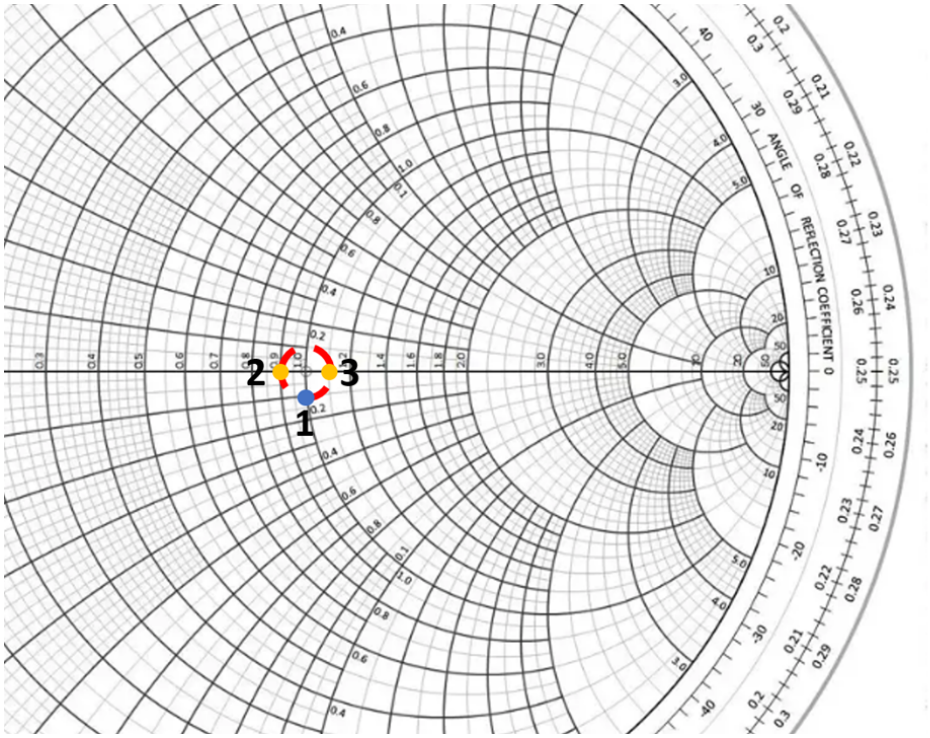

Figure 5.1: Smith Chart Used to determine Diode to Capacitor Spacing

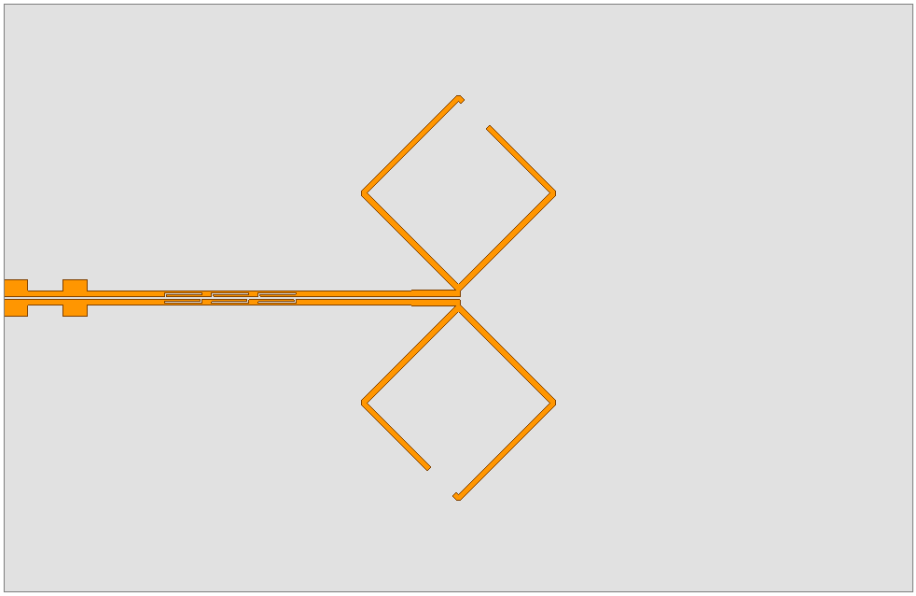

Figure 5.2: Final Rectenna Model in HFSS with Pads for Surface Mounted Components

Figure 5.3: Photo of Final Rectenna with Diode, Capacitor and Resistor Soldered

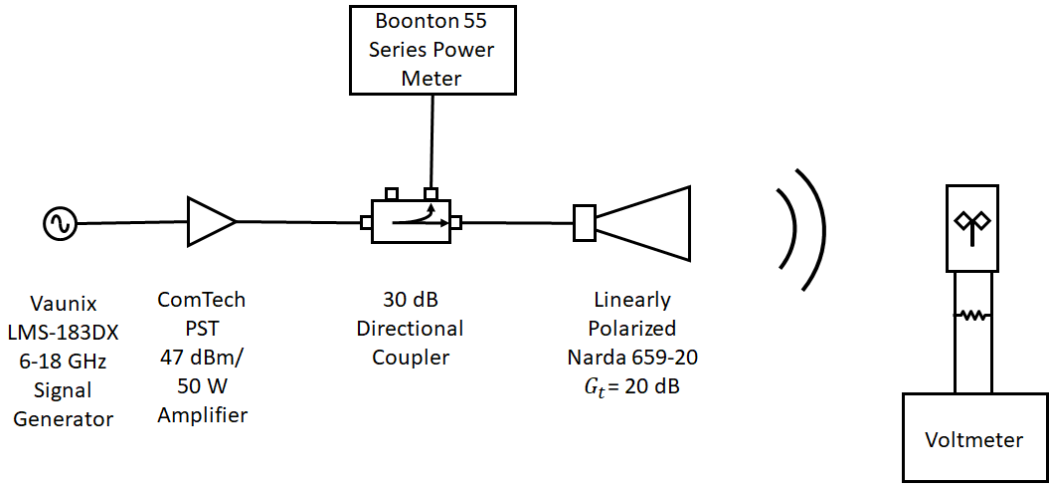

Figure 5.4: Rectenna Efficiency Measurement Setup

The rectenna was placed in a box with anechoic foam absorbers on all walls for the efficiency measurements. A Vaunix LMS-183DX 6-18 GHz signal generator was used to produce a continuous wave signal, amplified by a ComTech PST 50 W amplifier. A Boonton 55 Series Power Meter was used to read the power at the input of the Narda 659-20 horn antenna to track how much power is transmitted. Figure 5.4 shows a block diagram of the measurement setup and Figure 5.5 shows a picture of the setup. In order to keep as accurate account of the power transmitted through the horn antenna, the loss was measured through the cables and the directional coupler and it was less than 1 dB.

In order to obtain the rectenna's efficiency, linearly polarized energy is transmitted from the horn, to the rectenna. The rectenna is located a distance of 15 inches from the transmitting antenna. The rectenna's efficiency is simply the ratio of the converted DC power to the received RF power incident on the antenna as

$$\eta_R = \frac{P_{DC}}{P_{rec}} = \frac{4\pi s^2 \left(\frac{V_D^2}{R_L}\right)}{P_{trans} G_{trans} A_R^{eff} L_{pol}} \tag{5.1}$$

Figure 5.5: Photo of the Measurement Setup

where s represents the distance from the transmit horn to the rectenna, V_D represents the voltage across the resistive load, R_L represents the resistive load (250 Ω), P_{trans} represents the power transmitted, G_{trans} represents the gain of the transmit antenna, A_R^{eff} represents the aperture of the rectenna, and L_{pol} represents the polarization mismatch from the horn to the rectenna. The effective area of the rectenna is calculated as:

$$A_R^{eff} = \frac{\lambda_0^2}{4\pi} D_0 \tag{5.2}$$

where D_0 is the directivity or gain at broadside and λ_0 is the free-space wavelength of the incoming RF energy.

Since the horn antenna is linearly polarized, while the DRLA provides circular polarization, there is mismatch loss between the two represented by L_{pol}. The polarization mismatch can be calculated as:

$$L_{pol} = |\rho_w \cdot \rho_a{}^*|^2 = |\hat{a_x} \cdot \frac{1}{\sqrt{2}}(\hat{a_x} - j\hat{a_y})|^2 = \frac{1}{2} \tag{5.3}$$

where ρ_w represents polarization of the incoming linearly polarized wave emitted by the horn, and ρ_a represents the left hand circular polarization of the rectenna. Equation (5.3) says that half the transmitted energy will reach the rectenna due to polarization mismatch.

Figure 5.6 shows the measured vs. simulated efficiency curves for the rectenna. The simulated curves are generated from the rectenna model put forward by Yoo and Chang in [12]. The model predicts the efficiency to approach 81%, while the measured efficiency tops out at around 58%. The difference between the measured and calculated curves is due to several things not taken into consideration: 1) the harmonic effects of the diode are not taken into con-

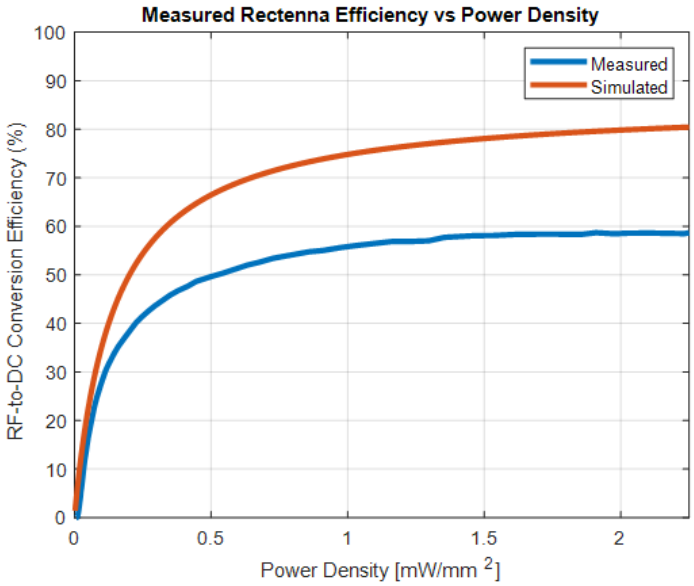

Figure 5.6: Rectenna Efficiency vs Power Density

sideration in the Yoo and Chang model; 2) the dielectric and conductor losses in the circuit were never measured; 3) difficulties in maintaining the proper space between the diode and capacitor due to the size of the flip chip diode.

Chapter 6

Rectenna Arrays

6.1 Array Operation Theory

If a large DC voltage is required, or the incident energy is much lower, arraying the rectenna can drive the diode to operate in its most efficient region. This is important as single element designs tend to require massive amounts of energy in order to push the diode past the "knee" voltage and into a forward biased state. In an array, the antenna element of the rectenna can be connected, either in series or parallel, with other antennas to combine the power they receive. This concept allows lower transmit powers (P_{trans} in equation (3.35)) to create larger diode voltages (V_D) which, in turn, increase the efficiency of the rectenna. It is important to note that the maximum efficiency of the rectenna system is set by the diode, and so arraying only allows the efficiency to be larger for a lower incident power density, and so the peak efficiency of the system is not necessarily changed. Arraying the antenna also increases the size of the aperture, but because of the direct squared relationship between V_D and η_R, the diode voltage has more of an effect.

There are two distinct manners in which rectennas can be arrayed, series and parallel. A model was put forward in [29] in which the authors studied

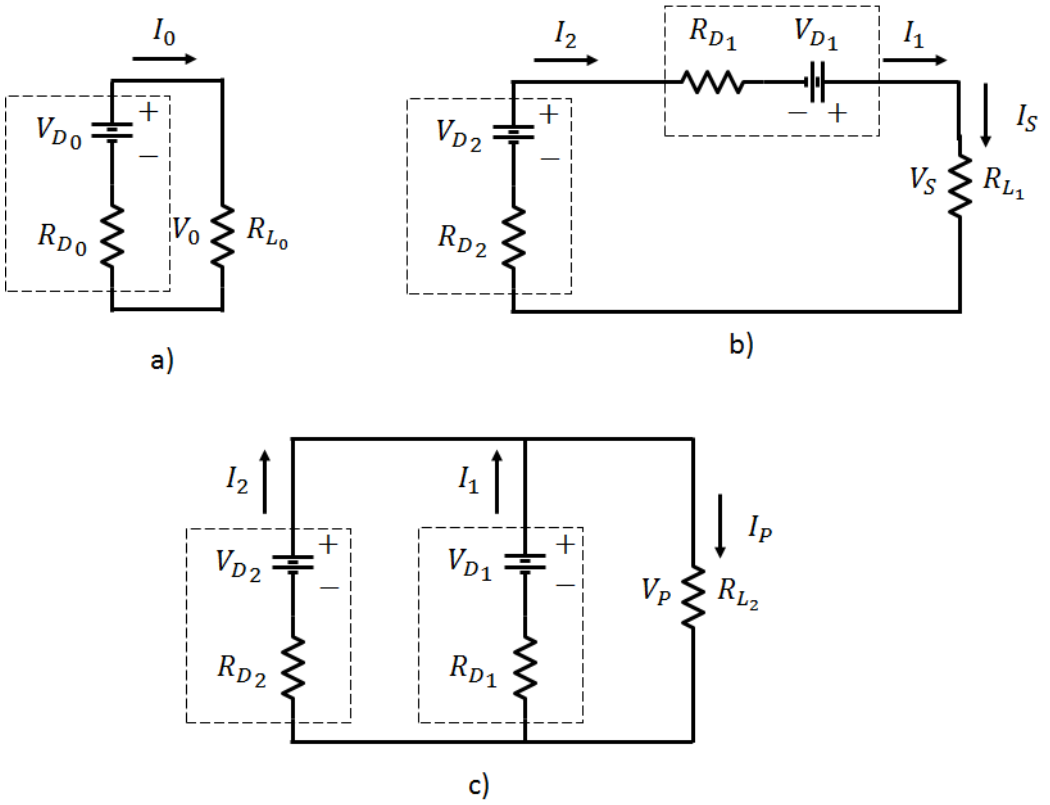

Figure 6.1: Equivalent Circuit Model of the Rectenna Arrays a) single element, b) series connection, c) parallel connection. V_{Di} and R_{Di} are equivalent voltage and resistances of the rectifying circuit. I_i and V_i are the current and voltage provided from the rectifying circuit to the output load. R_{Li} is the load resistance

each method. The equivalent model of the rectenna array is shown in Figure 6.1.

Using the equivalent circuit model, the parameters of the single rectenna, series rectenna and parallel rectennas can be found. For the single element, they are expressed by:

$$I_0 = \frac{V_{D_0}}{R_{D_0} + R_{L_0}} \tag{6.1}$$

$$V_0 = \frac{V_{D_0} R_{L_0}}{R_{D_0} + R_{L_0}}; \tag{6.2}$$

$$P_0 = \frac{V_{D_0}^2 R_{L_0}}{(R_{D_0} + R_{L_0})^2} \tag{6.3}$$

For the series connection:

$$I_S = \frac{V_{D_1} + V_{D_2}}{R_{D_1} + R_{D_2} + R_{L_1}} \tag{6.4}$$

$$V_S = \frac{(V_{D_1} + V_{D_2}) R_{L_1}}{R_{D_1} + R_{D_2} + R_{L_1}} \tag{6.5}$$

$$P_S = \frac{(V_{D_1} + V_{D_2})^2 R_{L_1}}{(R_{D_1} + R_{D_2} + R_{L_1})^2} \tag{6.6}$$

Assuming all elements are the same, then we can let $R_{D_1} = R_{D_2} = R_{D_0}$ and $R_{L_1} = R_{D_1} + R_{D_2} = 2R_{L_0}$. For maximum output power, the series connection parameters become:

$$I_S = \frac{V_{D_1} + V_{D_2}}{2\,(R_{D_0} + R_{L_0})} = \frac{1}{2}(I_1 + I_2) \tag{6.7}$$

$$V_S = \frac{(V_{D_1} + V_{D_2})\, R_{L_0}}{(R_{D_0} + R_{L_0})} = (V_1 + V_2) \tag{6.8}$$

$$P_S = I_S V_S = \frac{I_1 + I_2}{2} \cdot (V_1 + V_2) \tag{6.9}$$

And similarly the circuit parameters of the parallel connection:

$$I_P = \frac{V_{D_1} + V_{D_2}}{R_{D_0} + R_{L_0}} = (I_1 + I_2) \tag{6.10}$$

$$V_P = \frac{(V_{D_1} + V_{D_2})\, R_{L_0}}{2\,(R_{D_0} + R_{L_0})} = \frac{1}{2}(V_1 + V_2) \tag{6.11}$$

$$P_P = I_P V_P = (I_1 + I_2) \cdot \frac{V_1 + V_2}{2} \tag{6.12}$$

It can be seen when comparing equations (6.9) and (6.12) the output power of both series and parallel arraying is equal. The key difference between the two methods is whether a higher output voltage is required, or a higher output current. The series array creates a higher output voltage, while the parallel array creates a higher output current.

For the DRLA rectenna, a cascaded array called the honeycomb lattice will be used, similar to that found in [30]. This array uses rectenna elements joined in series with one another as seen in Figure 6.2. The array spacing is determined mainly by the effective areas of each individual rectenna element, but also by the DC-pass filter placement. The capacitors (DC-pass filters) isolate the array elements, and also optimize the RF-to-DC conversion. The proper capacitor placement is found using a similar reactance-cancelling approach as in section 5.1. Under the state of zero reactance, the array is perfectly matched.

The proper array spacing can be found using the directivity of the antenna. With this information, the effective area of each antenna can be calculated using equation (5.2). This effective area can be approximated as circular in shape meaning

$$A_R^{eff} = \pi r^2 \tag{6.13}$$

where r is the radius of that circular area. Referencing Figure 6.2, each column in the array contains 5 rectennas separated by d_y and each column is separated

by d_x. Both d_x and d_y should be less than 2r. The idea is to minimize the area where effective area circles overlap, only overlapping to ensure the entire area of the array is covered by the an aperture.

In Figure 6.2, diodes are placed on the inner 9 elements, with the extra outer "columns" only being etched for mutual coupling effects (to better predict the performance of a larger array). Using the procedure from section 3.3 and equation (3.35) an optimal load resistance can be calculated for the array. The rectennas on each column produce DC currents that add together to the final current through the load for each column. Similarly, the voltages of each column are summed resulting in a voltage V_A across the load resistor R_A. The diodes are connected in parallel in each column, and the columns are connected in series.

The array's efficiency measurement is the same as before - it is the ratio of the converted DC power to the received RF power. It is defined as:

$$\eta_A = \frac{P_{DC}}{P_{rec}} = \frac{4\pi s^2 \left(\frac{V_A^2}{R_A}\right)}{P_{trans} G_{trans} A_A^{eff} L_{pol}}. \tag{6.14}$$

Ultimately, the honeycomb array offers a very simple array design methodology that allows for the most efficient use of area on the array to absorb the most incident RF energy. By connecting several rectennas in series with one another, the output DC voltage is summed in each column to allow for very low incident power densities to drive the diode of each rectenna element.

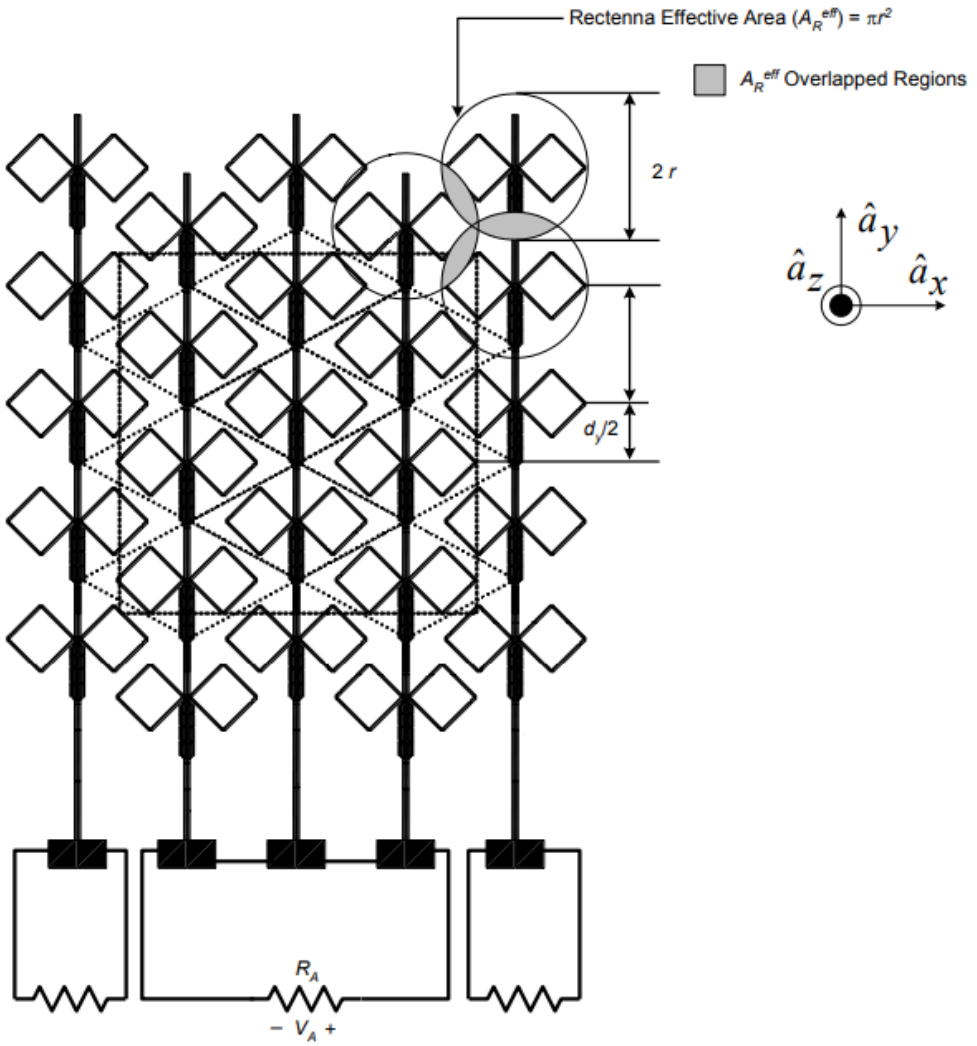

Figure 6.2: Array using a honeycomb lattice from [30]. Layout shows both rectenna and array effective areas along with all relevant spacings. The innermost 9 elements with the dotted unit cell areas represent the 3x3 array that rectifies the incident microwave energy. The remaining elements are present in order to account for the mutual coupling between adjacent rectenna elements. This allows the performance of the 3x3 array to predict the performance of larger arrays.

Chapter 7

Conclusion and Future Work

7.1 Conclusion

Harvesting clean and sustainable energy has become a goal of humanity in the modern era. The rectenna offers an efficient way to receive RF energy and convert it to usable DC power. It is a great alternative to heavy batteries and solar panels on space-based platforms because of its light weight, low cost and high-power handling capabilities. Traditionally, the rectenna has been implemented on thick rigid substrates using linearly polarized antennas. These types of rectennas offer great options for terrestrial wireless power harvesting; however, space bound systems should seek to be smaller, more flexible and light weight. The work presented here has improved on previous designs and laid out a procedure for realizing a circularly polarized rectifying antenna on a nonrigid substrate intended for use with satellite and other orbital power systems. The additional benefits of circular polarization for space based platforms are twofold: 1) the preservation of high output voltages regardless of orientation mismatch between transmit and receive antennas; 2) The detrimental effects of the ionosphere and the atmosphere on the propagation of electromagnetic waves can be ignored.

The demonstrated rectenna design was laid out on a 100 micron thick formable substrate with encouraging results. The diode used was the MACOM MA4E1317 flip-chip Schottky diode which was shown to have a maximum theoretical efficiency of 81% using the theoretical diode model derived by Yoo and Chang [12]. The designed rectenna showed an RF-to-DC conversion efficiency of 58% using a coplanar stripline architecture that employed a dual rhombic antenna and a spur-slot filter. The DRLA achieved an axial ratio of less than 1 dB at 10 GHz with more than 10°of spatial bandwidth and exhibited almost 7 dB of left-hand circularly polarized realized gain. Also presented in this work was a microstrip-to-CPS radial stub balun that saw very low insertion loss from 3 to 25 GHz. The balun also boasted a common mode rejection ratio of almost 25 dB. The final result was a fully flexible, high performance rectenna which displays very promising results for future implementation within SSPS systems.

7.2 Future Work

The RF-to-DC conversion efficiency of the proposed design achieved 58% while the proposed maximum efficiency the diode model predicted approached 81%. Several steps can be taken to increase the realized efficiency. A flexible mounting plane or fixture for the rectenna could be designed to ensure a $\lambda/4$ separation while maintaining the nonrigidity of the component. One suggestion in realizing such a mount is to use the same Pyralux substrate on a mechanical system that can bend and fold the rectenna with the use of a microcontroller.

A study should be conducted on the effect of distance on overall rectification efficiency as well. A distance of 15 inches from Tx to Rx was used to demonstrate the rectenna's performance, but this distance might be intro-

ducing some phase cancellation. Moving the rectenna closer and further away from transmit horn could have positive effects on the rectenna's capabilities. There is also a chance a plane wave may have not been incident on the rectenna due to the size limitations of the chamber used. More experiments should be conducted to verify the results.

An array of rectennas should be built according to the design procedure in chapter 6.1. Perhaps the biggest weakness of the rectenna is the dependence on very large transmit powers in order to drive the rectifier circuitry into an efficient region of operation. The easiest way to achieve a lower incident power density for high efficiency operation is to array the rectenna, which will allow the rectified voltage across several elements to combine into a much larger voltage seen by the load resistor.

The diode that was used for the rectenna was designed for low parasitics and high frequency operation. Since the diode is the heart of the rectenna system, research should always be conducted in solid state devices to achieve even lower parasitics to push the theoretical conversion efficiency of the diode ever higher.

It would also be prudent to investigate the possible combinations of the rectenna with other RF and electronic systems. The integration of the rectenna within a battery charging environment would be a good start as the only additional modification to the design would be the implementation of a voltage regulator to maintain a stable DC voltage on the output. More research could be conducted in the use of the rectenna system with communications systems or embedded sensors to achieve multi-purpose functionality.

Bibliography

[1] U. S. Energy Information Administration, *U.S. electricity generation by energy source*, `eia.gov/tools/faqs`, Last accessed on October 25, 2019.

[2] European Space Agency, *Space-based solar power*, `esa.int.gsp/ACT/projects/sps.html`, Last accessed on October 25, 2019.

[3] D. Wood, "Space-based solar power", Department of Energy, Ed., [Online]. Available: `energy.gov/articles/space-based-solar-power`.

[4] N. Tesla, "The problem of increasing human energy", *Century Magazine*, pp. 209–211, 1900.

[5] G Goubau and F. Schwering, "On the guided propagation of electromagnetic wave beams", *IRE Transactions on Antennas and Propagation*, vol. AP-9, pp. 248–256, 1961.

[6] W. C. Brown, "The history of power transmission and radio waves", *IEEE Transactions on Microwave Theory and Techniques*, vol. 32, pp. 1230–1242, 1984.

[7] W. C. Brown, "Experiments involving a microwave beam to power and position a helicopter", *IEEE Transactions on Aerospace and Electronic Systems*, vol. AES-5, pp. 692–702, 1969.

[8] W. C. Brown, R. H. George, N. I. Heenan, and R. C. Wonson, "Microwave to DC converter", pat. 3 434 678, 1969.

[9] P. E. Glaser, "Method and apparatus for converting solar radiation to electrical power", pat. 3 781 647, 1973.

[10] J. J. Schlesak, A. Alden, and T. Ohno, "Stationary high altitude relay platform - rectenna and low altitude tests", in *Global Telecommunications Conference*, GLOBECOM, Ed.

[11] J. O. McSpadden, L. Fan, and K. Chang, "Design and experiments of a high-conversion-efficiency 5.8-GHz rectenna", *IEEE Transactions on Microwave Theory and Techniques*, vol. 46, pp. 2053–2060, 1998.

[12] T.-W. Yoo and K. Chang, "Theoretical and experimental development of 10 and 35 GHz rectennas", *IEEE Transactions on Microwave Theory and Techniques*, vol. 40, pp. 1259–1266, 1992.

[13] B. Strassner and K. Chang, "5.8-GHz circularly polarized rectifying antenna for wireless microwave power transmission", *IEEE Transactions on Microwave Theory and Techniques*, vol. 50, pp. 1870–1876, 2002.

[14] W. C. Brown, "The technology and application of free-space power transmission by microwave beam", *Proceedings of IEEE*, vol. 62, pp. 11–25, 1974.

[15] W. C. Brown, "Recent progress in power reception efficiency in a free-space microwave power transmission system", *S-MTT International Microwave Symposium Digest*, 1974.

[16] A. S. Sedra and K. C. Smith, *Microelectronic Circuits 7th Ed.* 2015.

[17] J. O. McSpadden, *Rectenna technologies for SSP applications*, Huntsville, AL, 2018.

[18] Y.-H. Suh and K. Chang, "Coplanar stripline resonators modeling and applications to filters", *IEEE Transactions on Microwave Theory and Techniques*, vol. 50, pp. 1289–1296, 2002.

[19] E. Chen and S. Chou, "Characteristics of coplanar transmission lines on multilayer substrates: Modeling and experiments", *IEEE Transactions on Microwave Theory and Techniques*, vol. 45, pp. 939–945, 1997.

[20] W. C. Brown, "Electronic and mechanical improvement of the receiving terminal of a free-space microwave power transmission system", Raytheon Company, Technical Report.

[21] H.-K. Chiou and I.-S. Chen, "High-efficiency dual-band on-chip rectenna for 35- and 94-GHz wireless power transmission in 0.13 micrometer CMOS technology", *IEEE Transactions on Microwave Theory and Techniques*, vol. 58, pp. 3598–3606, 2010.

[22] Y.-H. Suh, C. Wang, and K. Chang, "Circularly polarised truncated-corner square patch microstrip rectenna for wireless power transmission", *IET Electronics Letters*, vol. 36, pp. 600–602, 2000.

[23] J. A. Hagerty and Z. Popovic, "An experimental and theoretical characterization of a broadband arbitrarily-polarized rectenna array", Phoenix, AZ.

[24] H Morishita, K Hirasawa, and T Nagao, "Circularly polarised wire antenna with a dual rhombic loop", *IEEE Proceedings - Microwaves, Antennas and Propagation*, vol. 145, pp. 219–224, 1998.

[25] R. N. Simons, N. I. Dib, and L. P. B. Katehi, "Modeling of coplanar stripline discontinuities", *IEEE Transactions on Microwave Theory and Techniques*, vol. 44, pp. 711–716, 1996.

[26] K. Goverdhanam, R. Simons, and L. P. B. Katehi, "Coplanar stripline components for high-frequency applications", *IEEE Transactions on Microwave Theory and Techniques*, vol. 45, pp. 1725–1729, 1997.

[27] Y.-G. Kim, D.-S. Woo, and Y.-K. Cho, "A new ultra-wideband microstrip-to-CPS transition", in *IEEE/MTT-S International Microwave Symposium*, IEEE/MTT-S, Ed.

[28] Y.-H. Suh and K. Chang, "A wideband coplanar stripline to microstrip transition", *IEEE Microwave and Wireless Components Letters*, vol. 11, pp. 28–29, 2001.

[29] N. Shinohara and H. Matsumoto, "Dependence of DC output of a rectenna array on the method of interconnection of its array elements", *Scripta Technica Electrical Engineering in Japan*, vol. 125, pp. 9–17, 1998.

[30] B. Strassner and K. Chang, "Highly efficient C-band circularly polarized rectifying antenna array for wireless microwave power transmission", *IEEE Transactions on Antennas and Propagation*, vol. 51, pp. 1347–1356, 2003.